

Recent advances in photocatalytic hydrogen evolution with high-performance catalysts without precious metals

Wan Zhao ^a, Zhi Chen ^{a, **}, Xiuru Yang ^a, Xiaoxiao Qian ^a, Chunxi Liu ^a, Dantong Zhou ^a, Tao Sun ^a, Ming Zhang ^b, Guoying Wei ^a, Pavani Dulanja Dissanayake ^c, Yong Sik Ok ^{c, d, *}

^a College of Materials and Chemistry, China Jiliang University, 258 Xueyuan Street, Xia Sha Higher Education District, Hangzhou, 310018, China

^b Department of Environmental Engineering, College of Quality & Safety Engineering, China Jiliang University, 258 Xueyuan Street, Xia Sha Higher Education District, Hangzhou, 310018, China

^c Korea Biochar Research Center, APRU Sustainable Waste Management & Division of Environmental Science and Ecological Engineering, Korea University, Seoul, South Korea

^d Sustainable Minerals Institute, University of Queensland, Brisbane, Australia



ARTICLE INFO

Keywords:

H₂ evolution
Solar energy utilization
Photocatalyst
Non-precious metal catalyst
Water splitting
Affordable and clean energy

ABSTRACT

The exploitation of green and renewable energy sources is imperative due to the environmental pollution produced by the massive use of non-renewable fossil energy. Hydrogen is a promising clean fuel since it exhibits high energy density and causes no secondary pollution. The photocatalytic production of H₂ from water splitting has gained immense attention since it is a low-cost, low-energy consuming, and environmentally friendly process. Various attempts have been made to prepare active and highly efficient catalysts for photocatalytic H₂ evolution. However, the use of precious metals as co-catalysts makes the H₂ production costly, thus limiting their practical applications. Herein, we discuss the latest advancements in the H₂ evolution on photocatalysts without noble metals. The progress achieved in the development of diverse photocatalysts has been critically evaluated in this review. Special attention has been paid to the challenges and tactics about enhancing the H₂ evolution upon non-noble-metal photocatalysts. This review will be helpful for designing high efficiency photocatalysts for fundamental research and practical applications.

1. Introduction

The energy crisis and environmental pollution caused by carbon-based fuels have attracted immense attention [1], which are detrimental to the ecosystem [2]. The development of renewable and eco-friendly energy sources that can replace traditional non-renewable sources has gained significant academic and industrial attention. Owing to its high energy density of 143 kJ g⁻¹, H₂ is considered as a promising clean energy source [3]. Moreover, it does not produce any secondary pollution.

There are three main strategies to produce H₂: H₂ evolution from fossil fuels, biofuels, and water splitting [4]. Currently, H₂ evolution from fossil fuels is the most popular approach, which includes methane reforming, natural gas pyrolysis, coal vaporization, and heavy oil partial oxidation. Methane reforming is a widely used technique for H₂

evolution and is cost-effective. However, it consumes a large amount of energy, and the reaction progresses as follows:



Moreover, finally produced CO₂ may cause greenhouse effect, resulting environmental problems [5]. Biological H₂ evolution involves the pyrolysis or gasification of biomass, fermentation of organic matter, photosynthetic bacteria breakage of organic matter, etc. [6,7]. The process is renewable and has very little harmful impact on the environment. These characteristics make this process suitable for civilian use. However, large-scale H₂ production using this approach is costly. H₂ production from water splitting is an eco-friendly approach, which utilizes wastewater as the source. Depending upon the resource used, the

** Co-corresponding author. College of Materials and Chemistry, China Jiliang University, Hangzhou, China.

* Corresponding author. Korea Biochar Research Center, APRU Sustainable Waste Management & Division of Environmental Science and Ecological Engineering, Korea University, Seoul, South Korea.

E-mail addresses: zchen0@gmail.com (Z. Chen), yongsikok@korea.ac.kr (Y.S. Ok).

processes of water splitting can be classified as photochemical, thermochemical, and electrochemical [8].

Since the first report of H₂ evolution on TiO₂ single crystal electrodes using photoelectrochemistry in 1972 [9], photochemical H₂ evolution from water splitting has been a constant hot spot both for academic and industrial interests. Depending upon the reaction mechanism, photochemical H₂ evolution can be classified into two main processes: photoelectrocatalytic and photocatalytic H₂ evolution. Along with light irradiation, the photoelectrocatalytic method uses photocatalysts as electrodes, which require an additional bias voltage to suppress the recombination of the photogenerated carriers. Photoelectrocatalytic H₂ evolution is widely used owing to its high efficiency. However, it requires additional energy, and hence will not be discussed in detail in this review. On the contrary, photocatalysis directly uses the abundant solar energy to split water into H₂ through a four-electron or two-electron process, which can effectively avoid environmental pollution and the consumption of extra energy. It is the simplest route for water splitting and provides low-cost and large-scale H₂ production. The recent publication trend of the reports focusing on the photocatalytic generation of H₂ is shown in Fig. 1. It can be clearly observed that the number of studies focusing on the development of photocatalysts without noble metals (denoted as non-noble metal photocatalysts) has increased significantly over the past few years. However, they are still less in number than those on the photocatalysts containing noble metals (named as noble-metal photocatalysts). Noble metals may work generally as the effective redox co-catalysts due to their excellent physico-chemical properties, electrical properties and high catalytic activities [10,11]. Nevertheless, noble-metal photocatalysts are costly because of the low abundance of the noble metals present in them, and hence find limited practical applications in water splitting. On the other hand, non-noble-metal photocatalysts are promising candidates for water splitting because of their low cost and good efficiency. In addition, non-noble metal photocatalysts exhibit good stability, and hence do not suffer from deactivation under specific conditions unlike Pt-based photocatalysts (noble-metal photocatalysts), which suffer from Pt deactivation in the presence of halide ions. This makes non-noble metal photocatalysts suitable for the conversion of wastewater to H₂. However, despite the above merits, very few reviews are available on the photocatalytic generation of H₂ using non-noble metal photocatalysts. In addition, the strategy for improving the H₂ production efficiency of non-noble metal photocatalysts needs to be investigated systematically.

This review mainly focuses on photocatalytic water splitting H₂

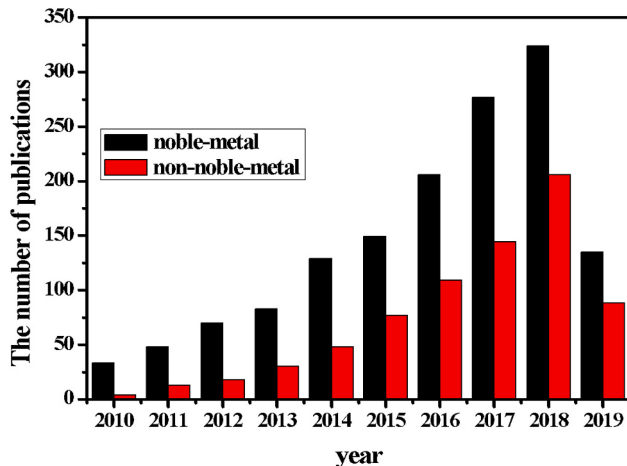
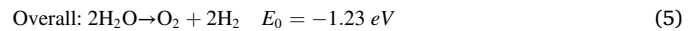
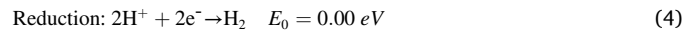
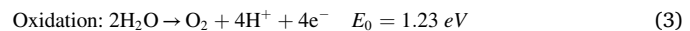


Fig. 1. Publications on the photocatalytic H₂ evolution using non-noble-metal and noble-metal photocatalysts since 2010 obtained by searching with keywords “photo or light”, “hydrogen or H₂ or H-2”, “non-noble metal or non-precious metal or precious metal free or noble metal free” or “noble metal or precious metal” (Adapted from Web of Science Core Collection: April 29, 2019).

production, and pay intense attention to the latest advances in H₂ production on non-noble metal photocatalysts such as metal oxides (TiO₂, etc.), metal sulfides (CdS, etc.), metal phosphides (NiP, etc.), and metal-free materials (g-C₃N₄, etc.). The strategies used for controlling and enhancing the efficiency of photocatalytic H₂ production are discussed. Finally, the current and future challenges in the production of H₂ on non-noble metal photocatalysts as well as the outlooks for their potential applications are described. This review provides an insight into the design of high-efficient and inexpensive photocatalysts for solar energy utilization and will create a pathway for the potential conversion of waste into H₂.

2. Fundamentals of photocatalytic H₂ production

It is reported that all the lanthanides and other elements in the s, p, and d regions of the periodic table can be used to produce H₂ [12]. The process of photocatalytic H₂ evolution can be divided into three successive stages: (1) the electrons in the valence band (VB) are excited and transmitted to the conduction band (CB) when the semiconductor absorbs high-energy photons greater than the bandgap, simultaneously generating holes in the VB; (2) the induced electron-hole pairs separate and transfer to the surface of the material; (3) the electrons in the CB reduce the adsorbed H⁺ to H₂ and the holes in the VB oxidize water into oxygen. However, a prerequisite must be met for H₂ production according to the following redox reactions [8]:



Under the Normal Hydrogen Electrode (NHE), the CB energy level should be lower than 0 V (E(H⁺/H₂)) for the occurrence of the H₂ evolution reaction (HER). In addition, the VB energy level should be higher than 1.23 V (E(O₂/H₂O)) for the occurrence of the reduction reaction of H₂O [13].

H₂ generation on non-noble metal photocatalysts is mainly restricted by their poor visible light response, fast recombination of the photo-generated carriers, low surface reaction rate, and high thermodynamic potential barriers. Various approaches such as energy band engineering, heterojunction construction [14], and reactive activity enhancement [15] have been used to overcome the above limitations. Immobilizing the co-catalyst on semiconductor photocatalysts is a promising approach to overcome the above mentioned limitations. Co-catalysts are classified as metallic, non-metallic, and semiconducting according to the category of material. Metallic co-catalysts can further be classified into precious metal and non-noble (base) metal catalysts depending upon the cost of the metal [5]. Over the past few decades, noble metals such as Ru [16], Rh [17], Pd [18], Ag [19], Pt [20], and Au [21] have been widely used as efficient co-catalysts for H₂ production. The addition of precious metal co-catalysts can vividly augment the activity of the photocatalyst. However, the use of noble-metal co-catalysts is not suitable for large-scale applications because of the high cost involved and limited storage. Therefore, the development of high-performance photocatalysts containing non-precious metals is an effective approach for sustainable and large-scale production of H₂ from water splitting. The non-noble-metal photocatalysts for H₂ production in this review are summarized in Table 1.

3. Non-precious metal photocatalysts for photocatalytic H₂ evolution

In this review, we have discussed various non-noble-metal photocatalysts such as metal oxides (TiO₂, etc.), metal sulfides (CdS, etc.), metal phosphides (NiP, etc.), and metal-free catalysts (g-C₃N₄, etc.). Diverse methods such as elemental doping, constructing

Table 1Summary of photocatalytic H₂ evolution based on non-noble-metal catalysts

Categories	Catalysts	Co-catalysts	Merits	Limitations	H ₂ evolution rate (μmol·h ⁻¹ ·g ⁻¹)	Ref
Metal oxide	TiO ₂	Doped N	Reduced microcrystalline rate and band gap	Low light absorption	1800	[22]
		Doped S	Reduced particle size, increased special surface area, improved light capture	Hydrogen production activity reduced by sulfur ions	800	
		Doped high-content C	Improved lifetime of photogenerated carriers, widened the light absorption range	Expensive raw materials	33.04	[23]
		Doped I and N	Inhibited recombination of photogenerated carriers, reduced band gap	Not experimental H ₂ production	/	[24]
		Doped Fe and Ni	Widened light absorption range, improved electron-hole separation efficiency	An alcohol solvent is necessary for H ₂ production	361.64	[25]
		Doped Fe ³⁺ and p ⁵⁺	Enhanced charge separation	Narrow visible-light-response range	724	[26]
		Loaded NiO	Reduced band gap energy, more exposed area of TiO ₂	Glycerin is the main source of H ₂ production	1230	[27]
		Incorporated CdS	Synergistic effect with TiO ₂	Additional sacrificial agents are required	2680	[28]
		Loaded CdS QDs	Reduced absorbed energy, improved material stability	Complicated preparation process is	1.89 μmol h ⁻¹ cm ⁻²	[29]
		Coated 1 T-MoS ₂	Inhibited charge recombination, enhanced long-term durability	Easy conversion of 1 T-MoS ₂ into 2H-MoS ₂	21,500	[30]
3	ZnO	Loaded NiS	Promoted fast carrier transport, more active sites	limited reported examples	7486	[31]
		Loaded Cu	Inhibited electron-hole recombination	No H ₂ production on TiO ₂ without Cu	283	[32]
		Doped S	Increased surface area, enhanced light capture	Complex preparation process	3640	[33]
		Doped Y and Al	Improved light absorption and stability, boosted electrons transfer	Crystal size increases with the increase of Y	5710	[34]
		Loaded g-C ₃ N ₄ NSs	Improved visible-light absorption and charge carrier separation, extended carrier life	Narrow visible-light-response range	322	[35]
		Coated MoS ₂	Favored charge transfer, inhibited electron-hole recombination	Only responds to ultraviolet light	768	[36]
		Loaded CdS QDs	Promoted photogenerated electron-hole separation and migration, inhibited electron-hole recombination, improved stability	High demand for morphology	22,120	[37]
		NiO	Increased active sites	Photosensitizer is necessary	7757	[38]
		Co ₃ O ₄			5552	
		Mn ₃ O ₄			196	
Metal sulfide	CdS	Loaded Ni ₃ C NPs	Increased visible light absorption, promoted carrier separation and transfer, improved surface H ₂ production kinetics	Poor cycling stability	18,020	[39]
		Loaded Co ₃ O ₄	Formation of p-heterojunction, enhanced light capture, charge transfer and separation capabilities	No H ₂ production compounded with P25, no stability test	3014	[40]
		Loaded TiO ₂	Formation of Z-scheme structure, promoted electron-hole separation	Limited cycles stability tests	1028	[41]
		Loaded MoS ₂ /graphene	Synergetic effects, inhibited charge recombination	Complicated preparation process	1913	[42]
		ZnS	Improved visible light absorption	Low oxidation potential	973.1	[43]
		Doped Cu	Improved visible light absorption, enhanced photogenerated charge transfer and carrier separation	Photocatalytic H ₂ production is not as effective as electrocatalysis	752.7	[44]
		Doped In and Cu	Plentiful active sites, effective electron-hole separation	Narrow visible-light-response range	301.25	[45]
		Loaded ZnO/g-C ₃ N ₄	Synergistic effect, promoted carrier separation	Low H ₂ production rate under ultraviolet light	686,000	[46]
		CdS/ZnS	Increased active sites, optimized electrical conductivity	Dye sensitizers are needed	155.2 μmol h ⁻¹	[47]
		Zn _{0.30} Co _{2.70} S ₄	Increased optical absorption	Low cycling stability	1001.8	[48]
Metal phosphide	CoP	WP	Doped Mo	Sacrificial agents are needed	806.5	[49]
		NiP	Doped Mn		15,300	
		Doped Fe	Doped Fe		16,700	
		Doped Co	Tunable activity by adjusting the Fe/Ni ratio		17,000	
		Fe-Ni-P	Construction of heterojunction, promoted carrier separation and transfer, expanded visible-light-response range	Dye sensitizers are needed	20,400	[50]
Metal free	g-C ₃ N ₄	Cu ₃ P	Hybridized MoP	/	5420	[51]
		Doped N	Improved light harvesting, promoted photo-excited charge carrier separation and transfer, extended and delocalize π-conjugated system	Aromatic heterocycles contained	855	
		Doped O	Reduced band gap, improved light capture	No stability test	1280	[52]
		Doped B and F	Enhanced visible-light absorption by B doping, promoted photoelectron generation, transfer, and separation by B-F co-doping and post-activation	Complicated preparation process, narrow visible-light response range	348	[53]
		Doped P	Effective charge transfer	Reduced oxidation potential	7020	[54]

(continued on next page)

Table 1 (continued)

Categories	Catalysts	Co-catalysts	Merits	Limitations	H ₂ evolution rate (μmol h ⁻¹ g ⁻¹)	Ref
SIC	Hybrid Fe ³⁺ -TiO ₂		Enhanced visible-light response, promoted carrier separation, extended carrier lifetime	Narrow visible-light-response range	3748.46	[56]
	Doped CdS NPs		Improved carriers separation, increased surface area	Agglomeration and photocorrosion of CdS	216.48	[57]
	Loaded MoS ₂		Strengthened visible-light absorption	No cycling stability test	231	[58]
	Loaded Ni ₂ P		Improved carrier separation and stability	High temperature needed for preparation	82.5	[59]
	Loaded SnO NSs		Synergistic effect, plenty of active sites	No cycling stability test	471.8	[60]
	Loaded g-C ₃ N ₄		Promoted carrier separation, increased surface area, increased hydrophilicity	High temperature needed for synthesis	182	[61]
Other	Loaded Ni(OH) ₂		Rapid electron migration	Poor cycling stability	31.5	[62]
	Loaded Tb ₃ N ₅		Improved interface charge separation, reduced defect density	Higher defect density leads to increased recombination centers	201.3	[63]
	HTiO _x /CNFs	Loaded NiS QDs	More exposed surface active sites, effective paths for carrier transfer	High temperature needed for the synthesis	2530.7	[64]

heterojunctions, and enhancing the reactivity all can be used to enhance the efficiency of photocatalytic H₂ production [65,66]. The general route for boosting the activity of photocatalytic H₂ evolution is shown in modification Scheme 1.

3.1. Metal oxide-based photocatalysts

Metal oxide semiconductors have become the most sought-after photocatalysts since the discovery of the photoelectrocatalytic generation of H₂ on anatase titanium dioxide (TiO₂) in 1972 [9]. Apart from TiO₂, other metal oxide semiconductors (including ZnO) are used as high efficiency photocatalysts without noble metals.

3.1.1. TiO₂

As an n-type semiconductor material, TiO₂ has good chemical stability, biological inertness, good thermal stability, and non-toxicity. It crystallizes in three common crystal structures: anatase, rutile, and brookite. Anatase TiO₂ is the most widely used photocatalyst owing to its high efficiency and stability. However, it has a wide bandgap (3.2 eV), leading to limited visible light absorption and solar energy utilization. The fast recombination of photogenerated carriers is another disadvantage of anatase TiO₂, which limits its hydrogen yield [67].

Structural and morphological control is used to increase the light absorption and charge separation/transmission of TiO₂ photocatalysts. It can also increase the surface area and produce new active sites, thus improving their performance and stability. TiO₂ photocatalysts with diverse morphologies such as nanosphere (0-D) [68], nanowire or nanotube (1-D) [69], and nanosheet (2-D) [70] have been developed (Fig. 2). In addition, dye sensitization is another way to increase the efficiency of H₂ production since it can broaden the light absorption. Table 2 summarizes the photocatalytic H₂ evolution on TiO₂ by structural and morphological control as well as dye sensitization.

Elemental doping is another strategy to tune the H₂ generation rate of TiO₂. Taherinia et al. [22] successfully incorporated N and S atoms into TiO₂ adopting a sol-gel method. The ultraviolet-visible spectra of the catalysts revealed that the S-doped TiO₂ sample exhibited a narrower bandgap than the N-doped one, and hence improved visible light absorption although the catalytic activity is influenced by the presence of sulfur ions. Moreover, the photocatalytic efficiency of N-doped TiO₂ grew with an augment in the number of N atoms. The highest H₂ yield was obtained at the N-doping amount of 6 wt% [22]. Jia et al. synthesized a hierarchical structure of highly carbon-doped TiO₂ (HC-TiO₂) by low-temperature stripping of the MXene supernatant [23]. The resulting HC-TiO₂ showed a flower-like morphology with tightly packed petals. The improved photocurrent on HC-TiO₂ can be attributed to the increased lifetime of its carriers, which in turn improved its H₂ production efficiency. The H₂ generation rate on HC-TiO₂ was 8.9 times greater than that upon P25. It was found that a valence band tail was induced at high carbon contents, which narrowed the bandgap and enhanced the utilization of light for the HER [23]. Additionally, Niu et al. theoretically investigated I and N co-doped TiO₂ by density functional theory (DFT) and proposed the chemical reaction pathways of water splitting through the climbing nudged elastic band (cNEB) method [24]. They pointed out that I and N co-doping could not only restrain the recombination of the photogenerated carriers but also reduce the bandgap of TiO₂ [24]. Apart from binary non-metal elemental doping, binary metal-element Fe, Ni [25] co-catalysts have also been applied to boost the productivity of H₂ production on TiO₂. Metal/non-metal doping can tune the energy band configuration of TiO₂, thus improving the light utilization and electron transport. In addition, a synergistic effect may be induced by multi-elemental doping, which may further improve the photocatalytic behavior of TiO₂. Elemental doping mixed with metal and non-metal has also been used to improve the H₂ production efficiency of TiO₂. Xiao et al. co-doped TiO₂ nanocrystals with Ti³⁺ and P⁵⁺ using a shape-controlled reagent-free method. The as-obtained product showed an ultra-high H₂ generation efficiency of

$724 \mu\text{mol h}^{-1} \text{g}^{-1}$ [26]. The mixed doping approach induced a synergistic effect of metal and metalloid (non-metal), which improved the activity on TiO_2 .

Constructing heterojunctions is another effective approach to tune the photocatalytic behavior of TiO_2 by adjusting the light absorption and facilitating the charge separation/transfer at the interface. Coupling TiO_2 with co-catalysts including oxides, sulfides, and others has also been carried out [88–91]. Fujita et al. fabricated NiO/TiO_2 catalysts with high H_2 production efficiency by adding NiO/TiO_2 to an aqueous solution of glycerin [27]. The addition of NiO could reduce the bandgap of TiO_2 and improve its photocatalytic activity without changing its structure and surface area. The highest H_2 production was achieved at the NiO content of 2 wt% [27]. Li et al. synthesized titanate nanotubes (TNTs) with tunable pore sizes and successfully incorporated CdS into the tubes by a simple ion-synthesis method. The incorporation of CdS induced a synergistic effect, which significantly improved the H_2 evolution efficiency of TiO_2 . The CdS/TiO_2 composites showed a maximum apparent quantum efficiency of 43.3% under visible light [28]. Moreover, Chen et al. successfully loaded CdS quantum dots (QDs) onto the TiO_2 nanotube arrays (TNTAs) through successive ionic layer adsorption and reaction (SILAR) method [29]. Enhanced and tunable performance for photocatalytic H_2 generation was observed, and the maximum activity of H_2 production was $1.89 \mu\text{mol h}^{-1} \text{cm}^{-2}$ when TNTAs were deposited with CdS QDs for 15 cycles. Fig. 3 shows the schematic diagram for the fabrication of CdS/TNTAs and the corresponding transport route of photogenerated carriers.

Han et al. loaded few-layered 1 T- MoS_2 onto TiO_2 (001) nanosheets to produce a photocatalyst with reduced charge recombination and improved durability, resulting in increased photocatalytic activity of 31.9% comparing with pure TiO_2 (001) [30]. Huang et al. immobilized NiS on TNTs using a hot solvent method and the obtained H_2 yield was $7486 \mu\text{mol h}^{-1} \text{g}^{-1}$ at the 8 wt% NiS loaded sample, which is 79 times greater than that from single TNTs [31]. Paramasivan et al. investigated the H_2 generation on metal-loaded TiO_2 through introducing Cu , Pb , Sn , and Zn metal particles into a TiO_2 aqueous methanol solution [32]. It was found that only the copper-loaded sample could produce H_2 , and its activity was about 68 times greater than that of pristine TiO_2 .

3.1.2. Zinc oxide (ZnO)

In the 1930s, ZnO was mainly used in the rubber and paper industries [92]. With the modification of ZnO using semiconductors, its applications extended to photocatalysis. Owing to its strong charge transport capability, direct bandgap, easy crystallization, and anisotropic growth, ZnO is considered as one of the potential photocatalysts for H_2 production. The electron mobility of bulk ZnO is about $100 \text{ cm}^2 \cdot \text{V}^{-1} \cdot \text{s}^{-1}$, which is 10 times larger than that upon TiO_2 [93,94]. This indicates that the photogenerated carriers in ZnO can easily migrate to its surface, thus improving its photocatalytic activity. Nevertheless, ZnO suffers from poor solar light utilization, poor chemical stability, and a high photo-generated carrier recombination rate. Modification with highly efficient co-catalysts is an effective approach to adjust its photocatalytic

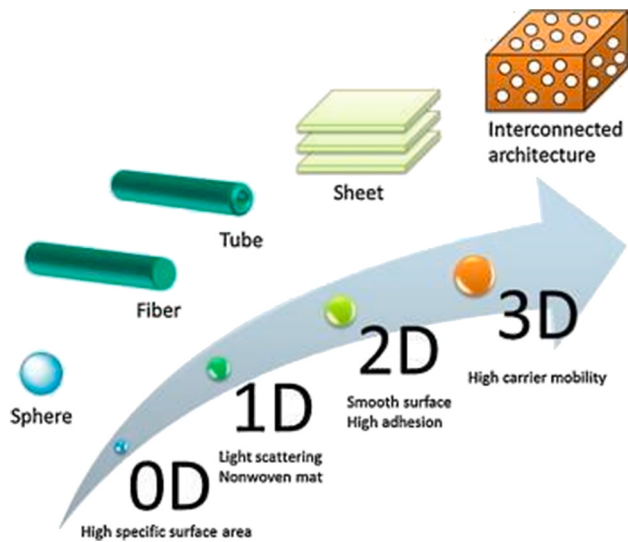
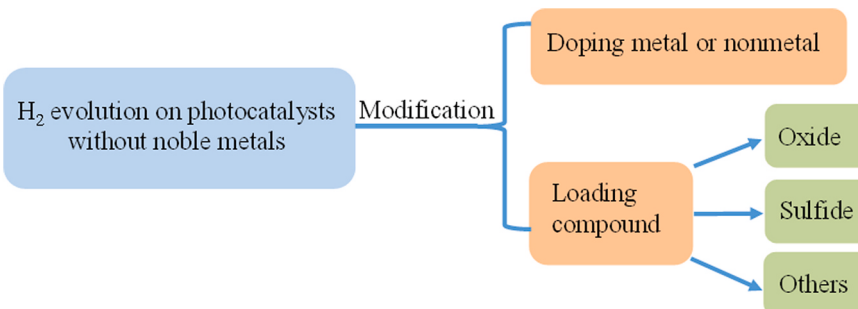


Fig. 2. Space structure of TiO_2 (Reproduced with the permission from the publisher [71]).

H_2 generation yield.

Elemental doping is another efficient route to boost the photocatalytic behavior of ZnO for H_2 generation. Various non-metallic (C, N, S, etc.), alkali metal (Li, Na, K, etc.), and transition metal (Cr, Mn, Cu, Co, Ni, Fe, etc.) elements have been used as dopants for ZnO [95]. Hsu and co-workers designed hierarchical S-doped ZnO photocatalysts for the HER and found that this special structure showed the high surface area and light trapping ability comparable to those ZnO nanorods. S-doped ZnO showed high stability even after five cycles, and the maximum H_2 generation yield was $3640 \mu\text{mol g}^{-1} \text{h}^{-1}$ [33]. Huo et al. prepared yttrium (Y) and aluminum (Al) co-doped ZnO (Y-AZO) through a sol-gel method. They found that 5%Y-AZO showed the best H_2 generation performance and an extremely high H_2 generation yield of $5.71 \text{ mmol h}^{-1} \text{g}^{-1}$ [34].

The introduction of additional components on ZnO to construct heterojunctions is a prominent approach to enhance its photocatalytic H_2 yield. Wang et al. fabricated core-shell $\text{g-C}_3\text{N}_4/\text{ZnO}$ (CN/OD-ZnO) heterojunctions by coupling $\text{g-C}_3\text{N}_4$ nanosheets with oxygen-deficient ZnO nanorods (OD-ZnO) and proposed the Z-scheme mechanism of electron transport in the photocatalysts [35]. As shown from the electrochemical impedance spectroscopy (EIS) results, the composite photocatalyst with 10 wt% $\text{g-C}_3\text{N}_4$ (CN-10/OD-ZnO) had the smallest diameter i.e., the lowest electron-transfer resistance (R_{et}). On the other hand, pure $\text{g-C}_3\text{N}_4$ showed the largest diameter i.e., the highest R_{et} . The heterojunctions significantly improved the electroconductivity of the ZnO , as shown in Fig. 4A. EIS is generally used to analyze the photocurrent response of a material. Accordingly, CN-10/OD-ZnO demonstrated the maximum photocurrent response, which was nearly eight



Scheme 1. A general strategy for photocatalytic H_2 evolution.

Table 2Summary of photocatalytic H₂ evolution on TiO₂ by structural and morphological control and dye sensitization

Photocatalysts	Light source	Solution	Type of TiO ₂	H ₂ evolution rate	Effect	Ref
TiO ₂	300 W Xe lamp ($\lambda \geq 420$ nm)	150 ml 10% v/v methanol and hexachloroplatinic acid	4–95 mol % anatase and the remaining is rutile; Nanoparticles	4250 ($\mu\text{mol h}^{-1} \text{g}^{-1}$)	Synergistic effect promotes the separation of photogenerated carriers	[72]
	AM 1.5 (100 mW/cm ²)	10 ml 50 vol% methanol	Anatase; Nanotubes	12 ($\mu\text{l h}^{-1} \text{cm}^{-1}$)	Structural defect engineering stimulates TiO ₂ activity	[73]
	100 W Hg lamp ($\lambda > 350$ nm)	100 ml 10 vol% methanol	Rutile; Three-dimensional; Facet heterojunction structure	1441 ($\mu\text{mol h}^{-1} \text{g}^{-1}$)	Extend the lifetime of photogenerated carriers	[74]
	500 W Xe lamp ($\lambda > 420$ nm)	Distilled water containing 20 vol% methanol	Nanotube arrays	2 ($\mu\text{mol cm}^{-2} \text{h}^{-1}$)	Expand surface area and increase active sites	[75]
	AM 1.5 (100 mW/cm ²)	100 ml 20 vol% methanol	Anatase; Ordered mesoporous	1362 ($\mu\text{mol h}^{-1} \text{g}^{-1}$)	Expand surface area, improve light-response range and stability	[76]
	UV-LED (380 nm)	9 ml 50 vol% methanol	Rutile;	900 ($\mu\text{mol h}^{-1} \text{g}^{-1}$)	Widen absorption range, 46% apparent quantum efficiency	[77]
	300 W Xe lamp	100 ml 10 vol% methanol	Anatase; Nanorods films	1874 ($\mu\text{mol m}^{-2} \text{h}^{-1}$)	Improve stability	[78]
	300 W Xe arc lamp ($\lambda > 300$ nm)	100 ml 10 vol% methanol	Anatase; Hollow microspheres	6600 ($\mu\text{mol h}^{-1} \text{g}^{-1}$)	Porous structure improves the photocatalytic properties	[79]
	AM 1.5 (100 mW/cm ²)	10 ml 50 vol% methanol	Anatase; Mesoporous nanoparticles	175 ($\mu\text{mol h}^{-1} \text{g}^{-1}$)	Specific defects improve photocatalytic properties	[80]
	300 W Xe lamp	20 vol% aqueous methanol	Anatase; Twinned nanocrystal	1272.66 ($\mu\text{mol h}^{-1} \text{g}^{-1}$)	Promote charge separation	[81]
6	300 W Xe lamp	50 ml methanol 220 mL H ₂ O	Brookite; nanosheets	8010 ($\mu\text{mol h}^{-1} \text{g}^{-1}$)	Higher conduction band potential for reduced hydrogen	[82]
AM 1.5	1 M NaOH		Anatase/rutile; Nanocrystalline	4.87 ($\mu\text{mol m}^{-2} \text{h}^{-1}$)	Increase surface area and crystallinity	[83]
1000 W Xe lamp	6 ml aqueous solution containing 4.28 mol l ⁻¹ of hole-scavenger		Anatase	1220 ($\mu\text{mol h}^{-1} \text{g}^{-1}$)	Longer lifetime of charge carriers	[84]
AM 1.5 G ($\lambda > 400$ nm)	25 vol% aqueous methanol		Anatase/rutile; Uniform ordered mesoporous microspheres	12,600 ($\mu\text{mol h}^{-1} \text{g}^{-1}$)	Large surface area and pore volume improve H ₂ production	[85]
AM 1.5 (100 mW/cm ²)	10 ml 50 vol% methanol		Anatase; Nanoparticles and nanotubes.	172 ($\mu\text{mol h}^{-1} \text{g}^{-1}$)	TiO ₂ can intrinsically activate H ₂ production under light	[86]
500 W Xe lamp	100 ml 50 vol% methanol		Anatase; Tapered tetragonal nanorods	703.4 ($\mu\text{mol h}^{-1} \text{g}^{-1}$)	Formation of heterojunctions between crystal planes to promote carriers separation	[87]

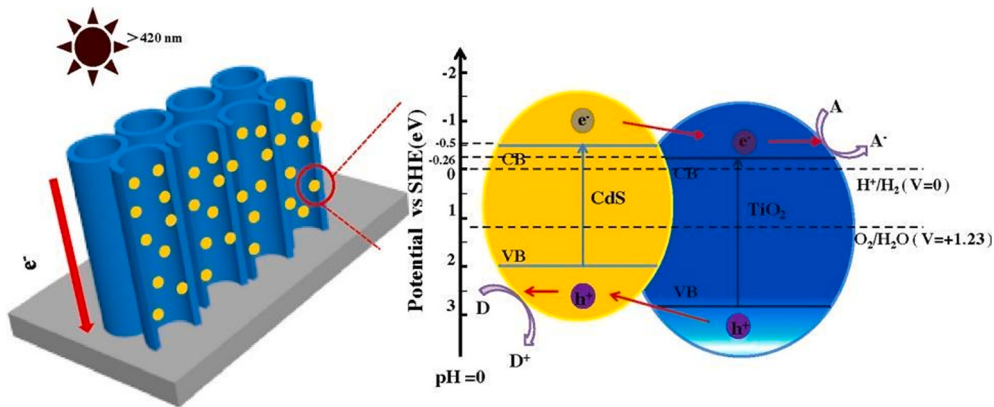


Fig. 3. Schematic diagram of H_2 generation on CdS-TNTAs (Reproduced with the permission from the publisher [29]).

folds greater than that upon $\text{g-C}_3\text{N}_4$ (Fig. 4B), due to its minimum R_{et} . Among the three characteristic heterostructures shown in Fig. 4C, the Z-scheme showed highly improved separation of the photogenerated carriers and the highest charge lifetimes, and hence the highest H_2 yield [35]. Yuan et al. synthesized a new MoS_2 nanosheet-coated ZnO heterojunction using a hydrothermal method [36]. They found that 1 wt% MoS_2/ZnO had the maximum H_2 generation rate of $768 \mu\text{mol h}^{-1} \text{ g}^{-1}$, which is 14.8 times greater than that on single ZnO . It may be mentioned that the HER photocatalytic activity of MoS_2 is greater than those on

precious metals including Pt or Au, demonstrating its potential to replace noble-metal co-catalysts. Ma et al. prepared a new CdS/ZnO heterostructure by combining 0-D CdS quantum dots (QDs) with 2-D ZnO nanosheets (NSs) [37]. $\text{CdS}/\text{ZnO}-12$ (12 is the deposition number of the CdS QDs) showed the maximum H_2 generation yield about $22.12 \text{ mmol h}^{-1} \text{ g}^{-1}$, which is 138 folds greater than that upon ZnO ($0.16 \text{ mmol g}^{-1} \text{ h}^{-1}$).

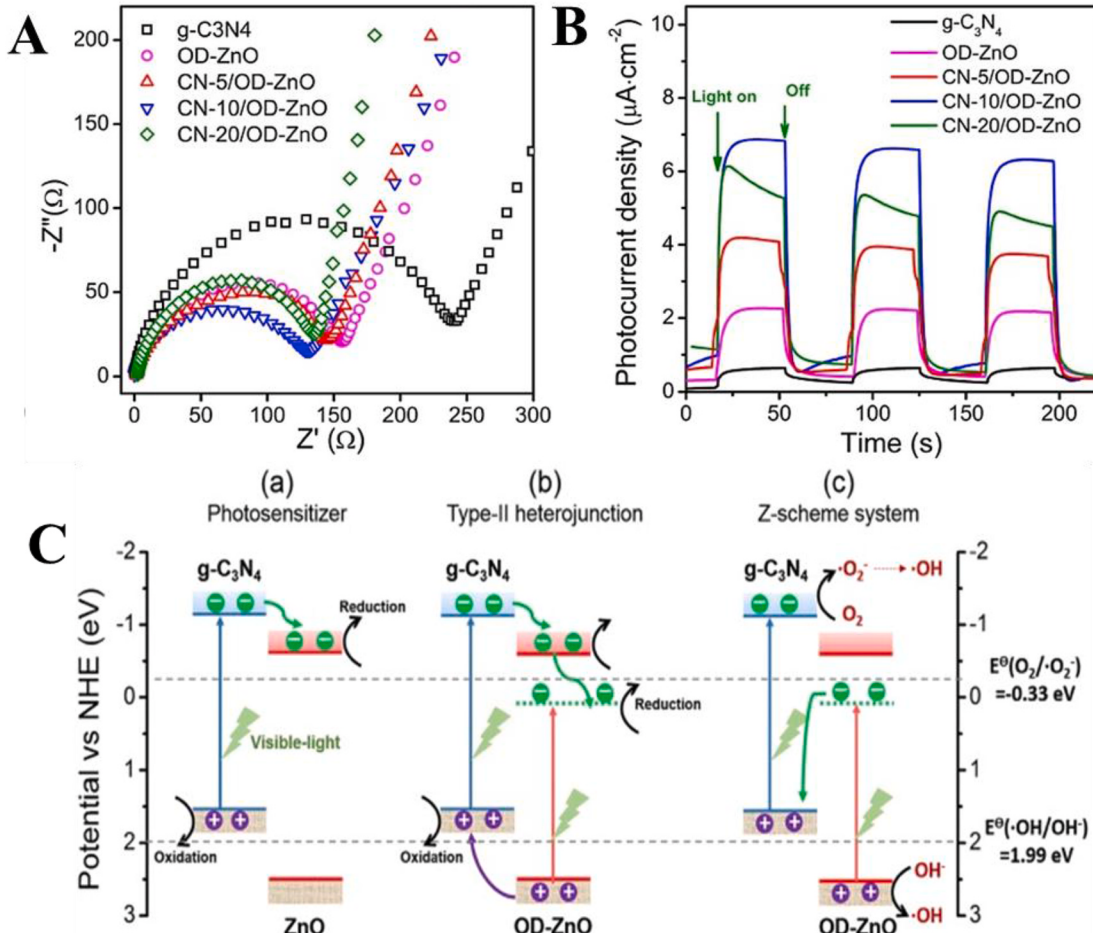


Fig. 4. (A) EIS results (B) photocurrent responses (C) $\text{g-C}_3\text{N}_4/\text{defect-free ZnO}$ (a), type II heterojunction of $\text{g-C}_3\text{N}_4/\text{OD-ZnO}$ (b), Z-scheme system of $\text{g-C}_3\text{N}_4/\text{OD-ZnO}$ (c) (Reproduced with the permission from the publisher [35]).

3.1.3. Other metal oxides

In addition, other metal oxides such as CuO, Fe₂O₃, and In₂O₃ have also been used for photocatalytic H₂ evolution. Yanalak et al. [38] designed a series of metal oxide nanofibers (NiO, Co₃O₄, and Mn₃O₄) for high-efficiency H₂ generation by using eosin-y (EY) as the photosensitizer and triethanolamine (TEOA) as the electron donor. The scanning electron microscopy (SEM) micrographs revealed that the NiO, Co₃O₄, and Mn₃O₄ nanofibers had diameters of 156 ± 10, 240 ± 10, and 140 ± 10 nm, respectively. The addition of the EY and TEOA co-catalysts improved the electron transfer of the nanofibers. The photocatalytic H₂ generation yield upon the NiO, Co₃O₄, Mn₃O₄ composite photocatalysts was 7757, 5552, 196 μmol g⁻¹ h⁻¹, respectively. The efficiency of the photocatalysts increased in the following order: Mn₃O₄ < Co₃O₄ < NiO. The H₂ evolution efficiencies of NiO, Co₃O₄, Mn₃O₄ nanofibers photocatalysts were higher than those of their bulk counterparts.

3.2. Metal sulfide-based photocatalysts

Metal sulfides are well-known photocatalysts for H₂ generation through water splitting. Metal sulfides are suitable for water reduction and exhibit better light response than oxides owing to their relatively high CB positions [96]. CdS (Eg = 2.4 eV) and ZnS (Eg = 3.6 eV) are the most investigated metal sulfide-based photocatalysts. However, metal sulfides photocatalysts suffer from photocorrosion, which may cause low stability. Strategies such as elemental doping and heterojunction construction have been used to improve their photocatalytic H₂ production efficiency.

3.2.1. Cadmium sulfide (CdS)

CdS shows two crystal phases: hexagonal wurtzite and cubic sphalerite. The CB and VB positions of CdS are -0.52 and 1.88 eV, respectively. The CB position of CdS is more negative than the H⁺/H₂ potential, while the VB position is more positive than the O₂/H₂O potential. Hence, CdS shows a large potential for H₂ evolution through water splitting. However, CdS photocatalysts suffer from two major disadvantages. They are highly susceptible to irreversible photocorrosion under irradiation, which seriously deteriorates their stability and limits their photocatalytic activity. The process of photocorrosion occurs as follows:



The other disadvantage is that they are deficient in active sites and exhibit low quantum efficiencies owing to the rapid recombination of photoinduced charges. Various co-catalysts were studied to adjust the H₂ production of CdS-based photocatalysts.

Ma et al. used Ni₃C nanoparticles as co-catalysts to modify CdS nanosheets for H₂ evolution by illuminating with a 350-W Xe lamp [39]. CdS-1%Ni₃C showed the largest H₂ generation yield about 450.5 μmol h⁻¹ in a 10 vol% lactic acid solution corresponding to a quantum yield of 8.72% at the wavelength of 420 nm, which is 4.79 multiples greater than that on bare CdS nanosheets. The article shows that the bandgaps of the CdS nanosheets and CdS-1% Ni₃C are 2.23 and 2.06 eV, respectively. The positive slopes of the Mott-Schottky (MS) spectra indicate that both the CdS nanosheets and CdS-1% Ni₃C were n-type semiconductors, and the CB positions (vs. Ag/AgCl) of CdS nanosheets and CdS-1% NiC were -1.07 and -1 V, respectively. Moreover, the VB position could be calculated using the formula: Eg = Ec - Ev. Lang et al. combined the p-type Co₃O₄ with an n-type CdS semiconductor to construct a CdS/Co₃O₄ p-n heterojunction, which displayed a high photocatalytic quantum efficiency of 9.4% [40]. Meng et al. successfully synthesized Z-scheme CdS/TiO₂ (Fig. 5) and achieved a H₂ evolution efficiency of 51.4 mol h⁻¹ [41].

Apart from binary complexes, ternary CdS-based photocatalysts with improved photocatalytic H₂ evolution have also been synthesized. Yu

et al. synthesized CdS/MoS₂/graphene hollow microspheres via a facile biomolecule-assisted self-assembly route and carried out photocatalytic H₂ evolution under visible light by employing an aqueous lactic acid solution as the sacrificial reagent [42]. The reaction rate on the composite photocatalyst with the MoS₂ content of 5% was 5 times larger than that on 1%Pt/CdS (Fig. 6A). The EIS results revealed that the CdS/MoS₂/graphene showed faster carrier transport than pure CdS because of its smaller diameter (Fig. 6C). The MS analysis of the photocatalysts revealed that both CdS and CdS/MoS₂/graphene were n-type semiconductors owing to their positive slopes, indicating that the flat band potentials (E_{FB}) were close to the CB of the semiconductors (Fig. 6D). CdS/MoS₂/graphene shows more negative E_{FB} (-0.99 V) than CdS (-0.88 V). This demonstrates that CdS/MoS₂/graphene exhibits a stronger redox potential which facilitates H₂ evolution. Moreover, the inserted graphene can augment the separation of carriers in CdS and improve the utilization of photogenerated electrons, as shown in Fig. 6E. In addition, the ternary system can also restrain the photocorrosion of CdS to some extent [42].

The strategies discussed thus far including the construction of binary, ternary, and Z-scheme systems can effectively improve the H₂ production and sustainability of CdS-type photocatalysts. However, the H₂ evolution reaction mechanism on CdS-based materials is still not clear and requires further investigation. The investigation of this mechanism will be helpful in designing novel powerful CdS-based photocatalysts.

3.2.2. Zinc sulfide (ZnS)

Similar to CdS, zinc sulfide (ZnS) is a direct bandgap semiconductor with a bandgap of 3.3–3.7 eV and shows two crystal structures: hexagonal wurtzite (α -ZnS) and cubic sphalerite (β -ZnS).

As a direct bandgap semiconductor material, ZnS shows high photon efficiency and excellent chemical and thermal stabilities. However, its wide bandgap (3.34 eV for sphalerite structure and 3.71 eV for wurtzite structure) and the fast recombination of photoinduced carriers restrain its applications in photocatalytic H₂ evolution. Various approaches such as elemental doping and heterojunction construction have been used to address the issues of ZnS photocatalysts. Lee et al. successfully synthesized Cu/ZnS microspheres using a microwave-irradiation method and found that 2 mol% Cu²⁺-doped ZnS displayed the maximum photocatalytic H₂ generation yield about 973.1 μmol h⁻¹ g⁻¹ [43]. They further synthesized In and Cu co-doped ZnS nanoparticles via using citric acid as the surfactant in deionized water and ethanol. The prepared samples were applied for splitting water to generate H₂ under simulated sunlight. The 4In4CuZnS photocatalyst exhibited the maximum H₂ generation yield of 752.7 μmol h⁻¹ g⁻¹ [43,44]. Dong et al. synthesized ternary ZnO/ZnS/g-C₃N₄ nanocomposites, a double Z-scheme heterojunction, by a simple two-step chemical conversion

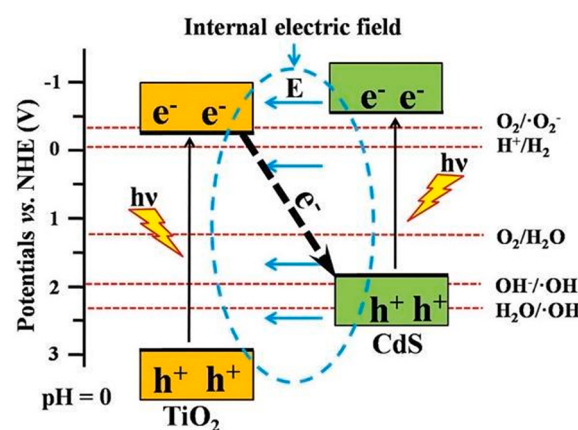


Fig. 5. Schematic of charge transfer in CdS/TiO₂ Z-scheme system (Reproduced with the permission from the publisher [41]).

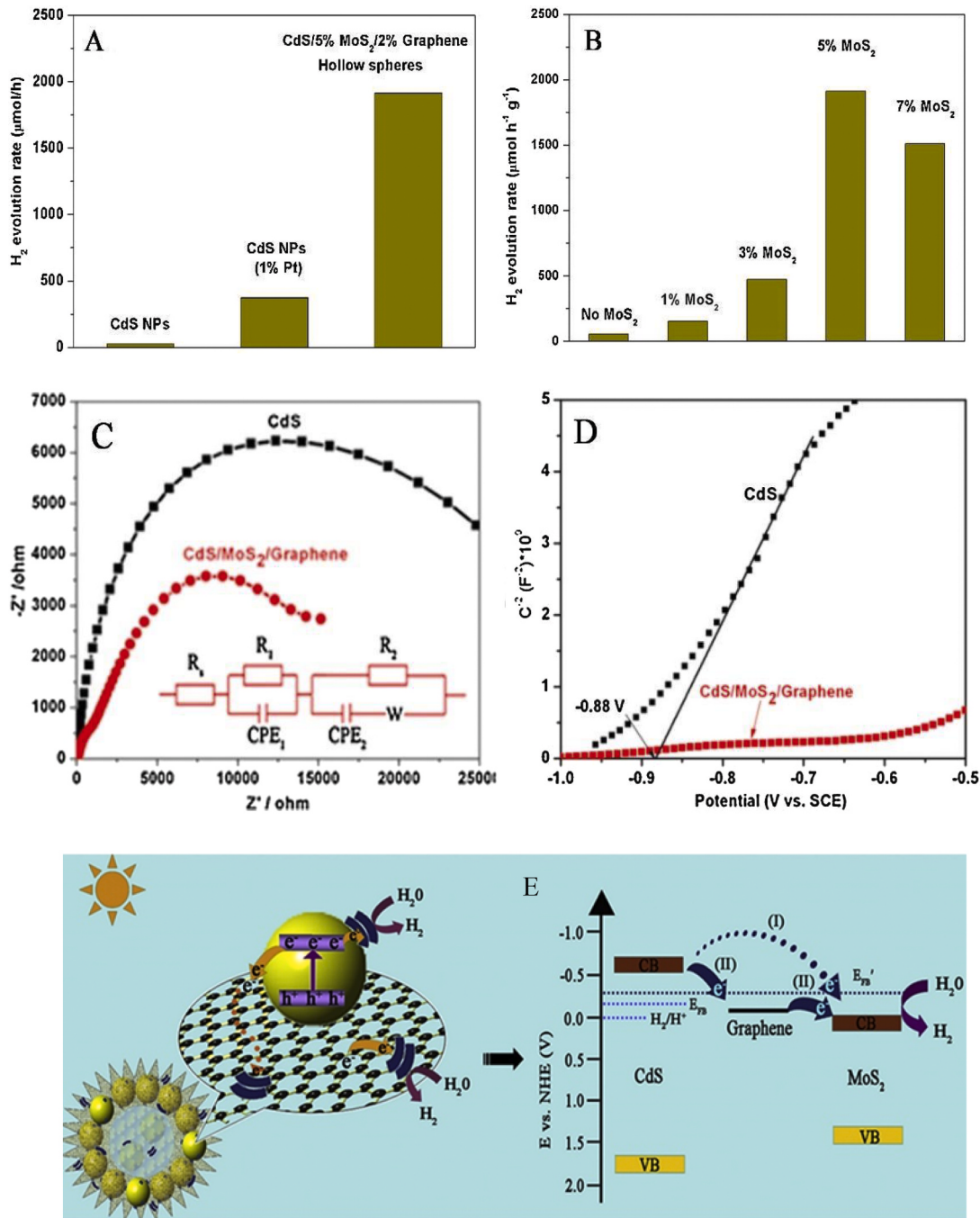


Fig. 6. (A) H₂ generation on CdS NPs, CdS/5% MoS₂/2% graphene hollow spheres, (B) H₂ evolution rates of CdS/MoS₂/graphene composites with different MoS₂ contents, (C) EIS results and (D) MS plots on CdS and CdS/MoS₂/graphene hollow sphere-modified electrodes, (E) Schematic of photocatalytic H₂ generation (Reproduced with the permission from the publisher [42]).

method. The ternary ZnO/ZnS/g-C₃N₄ nanocomposites showed abundant active sites and improved photocatalytic activity. A high H₂ generation rate of 1205 μmol g⁻¹ could be realized via water splitting after solar illumination for 4 h [45]. The modification strategies described above can effectively boost the light utilization, charge separation/transport, and active sites of ZnS-based photocatalysts, and hence can significantly improve their photocatalytic H₂ generation efficiency (from water splitting).

Reddy and co-workers developed an ultra-thin core/shell CdS/ZnS photocatalyst for H₂ evolution by adopting a one-step hydrothermal approach. The shell prevented the photo-corrosion of the core, and hence increased the stability of the core/shell CdS/ZnS photocatalysts

for constant H₂ generation. The activity of the core/shell CdS/ZnS photocatalysts was 763- and 2.4-folds greater than those of pristine CdS and ZnS, respectively. The core/shell CdS/ZnS photocatalysts showed a quantum efficiency of 8.78%. Moreover, the core/shell CdS/ZnS photocatalysts exhibited excellent stability even under 20-W LED light irradiation at 420 nm for 100 h [46].

3.2.3. Other metal sulfides

Like single-metal sulfides, multi-metal sulfides also show a tunable band energy structure, which can improve their light response and charge separation/transfer, and thus their photocatalytic H₂ production efficiency. Huang et al. fabricated hollow bimetallic sulfides (M_xCo₃-

xS_4 , M = Zn, Ni, Cu) through a facile self-template strategy. Compared to other sulfides, Co_3S_4 is a promising sulfide photocatalyst for the HER. Its photocatalytic behavior is significantly augmented by the addition of secondary homogeneous metallic elements such as Zn, Ni, and Cu. Especially, hollow $Zn_{0.30}Co_{2.70}S_4$ displays an excellent photocatalytic H_2 generation yield of $155.2 \mu\text{mol h}^{-1}$ when it is sensitized with EY. This H_2 generation activity is comparative to that on commercial Pt/C. Furthermore, $Zn_{0.30}Co_{2.70}S_4$ shows good stability under neutral or alkaline conditions [47].

3.3. Metal phosphide-based photocatalysts

Metal phosphides exhibit good mechanical stability, electron conductivity, and chemical stability. Metal phosphides show a crystal structure with a triangular prism configuration because of the large radius (0.109 nm) of P atoms. Metal phosphides tend to form isotropic crystal structures and contain a large number of unsaturated coordinated surface atoms, which may induce a high photocatalytic activity.

It has been reported that some metal phosphides such as MoP [97], Fe_2P , Ni_2P , Co_2P [98,99], and WP [100] work efficiently as co-catalysts to modify TiO_2 , CdS, and g-C₃N₄ photocatalysts. The incorporation of these metal phosphides induces a synergistic effect and improves the photocatalytic activity of TiO_2 , CdS, and g-C₃N₄. However, metal phosphides can serve as prominent photocatalysts by themselves for photocatalytic H_2 evolution. Li et al. synthesized pure CoP and WP with low crystallinity and excellent optical properties. The H_2 evolution kinetics revealed that H_2 could be continuously produced by water splitting for 60 h on 10 mg CoP and WP. The amounts of H_2 generated on CoP and WP were 601.1 and 483.9 μmol , respectively. Both the catalysts showed remarkable photocatalytic activity and stability [48].

Metal-doping has been employed to improve the photocatalytic H_2 generation efficiency of phosphide-based photocatalysts. Man et al. reported the doping of NiP with transition metal elements including Mo, Mn, Fe, and Co through a facile wet-chemical method. These transition metals can replace nickel atoms in the crystal to form NiMP (M = Mo, Mn, Fe, Co) without changing its structure and shape, which is evidenced from the TEM analyses (Fig. 7A and B). H_2 evolution rates of

15.3, 16.7, 17, 20.4, and 17.7 $\text{mmol h}^{-1} \text{g}^{-1}$ were observed for NiMoP, NiMnP, NiFeP, NiCoP, and Ni_2P , respectively, when EY was used as the photosensitizer [49], as shown in Fig. 7C.

Dye sensitization has also been introduced to promote the H_2 production on the phosphide-based photocatalysts. Li et al. [50] synthesized bimetallic Fe–Ni–P nanotubes through a metal-organic framework derived method and injected different dyes on the tubes. The dye-sensitized Fe–Ni–P nanotubes exhibited prominent photocatalytic H_2 production performance by coordinating the Fe/Ni ratio, and the maximum H_2 production rate of $5420 \mu\text{mol h}^{-1} \text{g}^{-1}$ was achieved at eosin-Y sensitized Fe-1-Ni-2-P [50].

To construct heterojunction is another route to suppress the electron-hole recombination. Song et al. prepared MoP–Cu₃P hybrids and the Schottky junctions were formed between intimate interfaces. The hybrids showed promoted features for visible-light harvesting, carrier separation and transfer, which resulted in an enhanced photocatalytic H_2 production of $855 \mu\text{mol h}^{-1} \text{g}^{-1}$ [51].

3.4. Metal-free photocatalysts

Since Wang et al. [101] reported the application of g-C₃N₄ for H_2 evolution from water splitting in 2009 for the first time, metal-free g-C₃N₄ photocatalysts have gained immense attention and have been widely used. SiC is another metal-free photocatalyst for the HER and the investigation of its photocatalytic properties can be traced back to 1990. Significant advances have already been made to improve the photocatalytic H_2 generation on SiC.

3.4.1. Graphite phase carbon nitride (g-C₃N₄)

Graphite phase g-C₃N₄ is a non-metallic organic semiconductor possessing a narrow bandgap of 2.7 eV. It has two chemical structures: triazine rings and 3-s-triazine rings. In addition, its conduction band is lower than the standard hydrogen electrode potential, which facilitates water splitting to produce H_2 .

Although g-C₃N₄ is considered as an efficient photocatalyst, it still suffers from a low specific surface area, wide bandgap, and fast recombination of electron-hole pairs, which restrain its practical

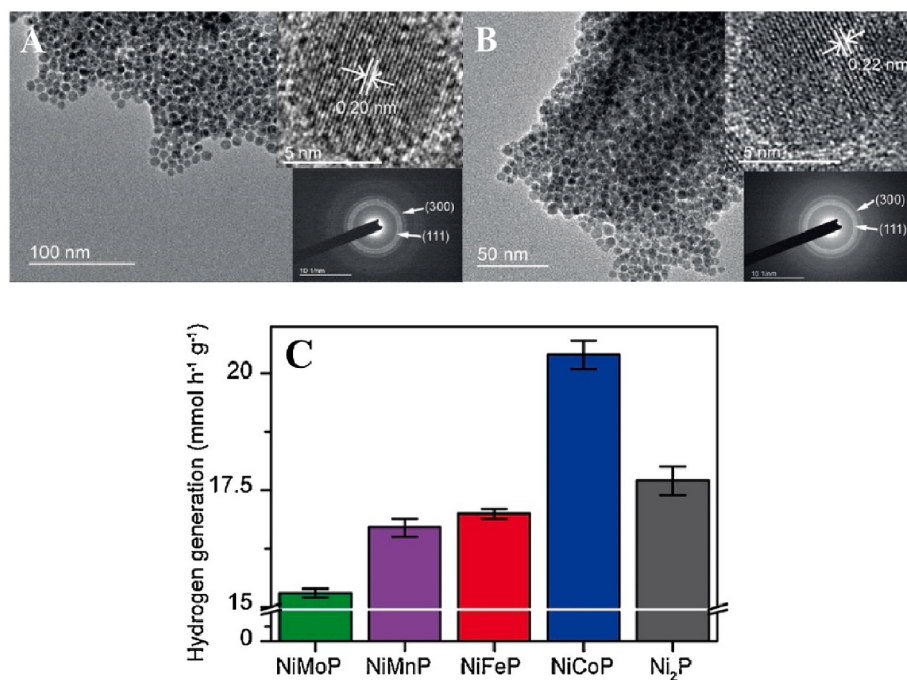


Fig. 7. (A) TEM micrographs of (A) Ni_2P , (B) NiMoP, (C) photocatalytic H_2 evolution effect induced by adding eosin Y as the photosensitizer into H_2O (Reproduced with the permission from the publisher [49]).

applications. Various modification methods such as morphology control, metal or non-metal element doping, and constructing heterojunctions are used to improve its photocatalytic properties.

Morphology control is an effective route to tune the intrinsic activity of g-C₃N₄, which in turn, can improve its H₂ evolution efficiency. As can be observed from Table 3, various g-C₃N₄ photocatalysts with diverse shapes have successfully prepared. These photocatalysts show distinct specific surface areas and exhibit different intrinsic activities, which significantly affect the rate of H₂ evolution.

Apart from morphology control, metal (Fe, Cu, and Zn, etc.) and/or non-metal (B, C, N, O, F, P, and S, etc.) doping has been investigated intensively to tune the photocatalytic behavior of g-C₃N₄. Zhou et al. synthesized N-doped graphitic carbon-incorporated g-C₃N₄ via thermal polymerization by adding urea and citric acid as the precursor [52]. The doped samples showed remarkably improved photogenerated carrier separation efficiency. The samples showed the highest H₂ generation rate of 64 μmol h⁻¹, which is 4.3 multiples larger than that of single-phase g-C₃N₄ [52]. Wang et al. prepared O-doped g-C₃N₄ photocatalysts by a one-pot solvothermal method [53]. With an increase in the dopant concentration, the bandgap of the photocatalyst decreased and the light utilization and charge separation improved. The highest H₂ yield obtained under visible-light irradiation was 348 μmol h⁻¹ g⁻¹. Cui et al. prepared B- and F-co-doped g-C₃N₄ photocatalysts through a simple two-step approach using [Emim]F-4 as the dopant [54]. B was doped in the internal framework of g-C₃N₄, which enhanced its visible light absorption and produced uniform porous structures after post-sintering. On the other hand, F was doped only on the surface layer. The photoelectron generation and separation of the g-C₃N₄ improved observably because of the synergistic effect of B and F doping. As a result, a good H₂ generation yield of 351 μmol h⁻¹ was achieved. Zhu et al. designed binary black phosphorus/graphite carbonitride (BP/g-C₃N₄) heterojunctions by introducing 2-D BP as the co-catalyst [55]. By strengthening the interfacial reaction, the charge transfer at the heterojunctions could be optimized, which efficiently improved their photocatalytic performance. The maximum H₂ release yield of 428 μmol g⁻¹ h⁻¹ was obtained at the optimal BP/g-C₃N₄ ratio of 1/4.

Other compounds with wide bandgaps have also been investigated to modify g-C₃N₄ for advancing its photocatalytic H₂ evolution performance. It should be noted that the photocatalysts obtained using this approach are different from the abovementioned g-C₃N₄ photocatalysts, in which g-C₃N₄ played as the co-catalyst. Yu et al. modified g-C₃N₄ with Fe³⁺-doped TiO₂ through a facile pyrolysis method [56]. The prepared composites exhibited significantly improved visible light response and photocatalytic performance. The maximum H₂ production of 3748.46 μmol g⁻¹ h⁻¹ was realized and the quantum efficiency at 400 nm reached 1.42% when the mass ratio of g-C₃N₄ and TiO₂ was 3:1. Cong et al. used an in-situ hydrothermal method to synthesize CdS/g-C₃N₄ nanocomposites containing a large surface area and improved charge separation [57]. A great photocatalytic H₂ evolution rate of 216.48 μmol h⁻¹ g⁻¹ was obtained at the optimal CdS amount of 10 wt%. Tian et al. prepared a new MoS₂/g-C₃N₄ heterostructure photocatalyst through a facile impregnation and calcination method by using cyanamide, ammonium molybdate, and thiourea as the precursors [58]. A H₂ generation yield of 23.10 μmol h⁻¹ was achieved under visible-light irradiation ($\lambda > 400$ nm). This H₂ generation rate was 11.3 folds than that obtained with pure g-C₃N₄. MoS₂/g-C₃N₄ heterojunctions can also

be prepared using the ion-exchange and hydrothermal method [105]. Ye et al. grew Ni₂P on the g-C₃N₄ surface by annealing, which facilitated the formation of a strong interface [59]. The prepared Ni₂P/g-C₃N₄ exhibited a super H₂ production rate of 82.5 μmol h⁻¹ g⁻¹, which is much larger than that obtained on Pt-loaded g-C₃N₄ under the same experimental conditions. The H₂ generation rates on different improved g-C₃N₄ samples are listed in Table 4.

3.4.2. Silicon carbide (SiC)

SiC is the only solid binary carbide in group IV with a strong sp³ hybrid covalent bond. The crystal units of SiC are tetrahedrons formed by four Si/C atoms and a C/Si atom at the center. Since the electronegativities of Si and C are different (Si = 1.8 and C = 2.6), the covalent bond between them is polarized, resulting in different bond lengths between Si-C and the adjacent carbon layers. This generates relatively low stacking fault energy in SiC despite its strong covalent bonds. As a result, SiC shows different shapes and more than 250 structures have been reported.

The application of SiC in photocatalysis can be traced back to 1990. Nariki, a Japanese researcher, used the arc-discharge method to produce various SiC nanopowders and used them for photocatalytic water splitting [128]. The reduction ability of SiC under UV irradiation is very strong and can be even an order of magnitude larger than that of Pt/TiO₂. Till date, various methods have been developed to generate H₂ from photocatalytic water decomposition on SiC based photocatalysts. Wang et al. fabricated a core-shell hierarchical architecture by growing ultrathin SnO₂ nanosheets on mesoporous SiC nanofibers through a facile hydrothermal method [60]. The H₂ evolution rate could reach 471.8 μmol h⁻¹ g⁻¹ under simulated sunlight. This good H₂ generation yield is ascribed to the production of a large number of active sites by the ultrathin SnO₂ nanosheets, hierarchical structure, and synergy of the SnO₂/SiC composite. Wang and co-workers employed an in-situ method to synthesize g-C₃N₄/SiC composites with tunable mass quantities [61]. First, the SiC powder was put into a thiourea solution and the resulting mixture was constantly stirred at 55 °C to completely evaporate deionized water. Finally, graphitic g-C₃N₄/SiC was obtained after heating the mixture at 550 °C for 2 h. The prepared g-C₃N₄/SiC exhibited high stability in the H₂ generation process and the highest H₂ yield reached 182 μmol h⁻¹ g⁻¹, which is 3.4 folds greater than that obtained on pure g-C₃N₄. The improved performance of g-C₃N₄/SiC is mainly ascribed to the following two aspects: one is the increased surface area, and the efficiently promoted separation and migration of the photoinduced carriers; the other is the increased polymerization degree of g-C₃N₄ and the improved hydrophilicity of SiC. However, the extensive application of SiC in photocatalytic H₂ evolution is limited and its modification with a suitable co-catalyst is still a challenge.

3.5. Other photocatalysts

The application of metal oxynitride as a photocatalyst was firstly reported by the scientists from Nippon Institute of Technology. TaON, a metal oxynitride, has a small bandgap of 2.5 eV and can respond to visible light. Furthermore, its CB potential is slightly negative than the standard hydrogen electrode potential and its VB potential is 2.2 V, which is sufficient for water decomposition [129,130]. Chen et al. used Ni(OH)₂ as the co-catalyst to modify TaON by loading Ni(OH)₂ on TaON

Table 3
H₂ evolution on g-C₃N₄ with different morphologies

Photocatalyst	Illumination (Xe Lamp)	Specific surface area (m ² ·g ⁻¹)	H ₂ evolution rate (μmol·h ⁻¹ g ⁻¹)	Ref.
g-C ₃ N ₄ bulk	300 W	7.56	302	[102]
g-C ₃ N ₄ Nanosheet	300 W	43.81	625.8	[102]
3D open porous g-C ₃ N ₄	300 W	37	1590	[103]
g-C ₃ N ₄ Nanotube	300 W	85.50	633	[104]

Table 4H₂ generation on modified g-C₃N₄

Photocatalyst	Incident light (λ)	Solution	H ₂ evolution rate ($\mu\text{mol}\cdot\text{h}^{-1}\cdot\text{g}^{-1}$)	Ref.
TiO ₂ /g-C ₃ N ₄	300 W Xe lamp with a solar filter	25 ml 20 vol% methanol	1960	[106]
CoO/g-C ₃ N ₄	LED ($\lambda > 400$ nm)	20 ml pure water	50.2	[107]
Cu ₂ O/g-C ₃ N ₄	300 W Xe lamp ($\lambda > 400$ nm)	100 ml aqueous solution containing 20 ml TEOA	33.2	[108]
Cr ₂ O ₃ /g-C ₃ N ₄	300 W Xe lamp ($\lambda > 420$ nm)	200 ml 20 vol% TEOA	109	[109]
Nb ₂ O ₅ /g-C ₃ N ₄	300 W Xe lamp ($\lambda > 420$ nm)	100 ml 10 vol% TEOA	1710.04	[110]
Ta ₂ O ₅ /g-C ₃ N ₄	300 W Xe lamp ($\lambda > 420$ nm)	200 ml 20 vol% methanol	36.4	[111]
CeO ₂ (110)/g-C ₃ N ₄	300 W Xe lamp ($\lambda \geq 420$ nm)	100 ml 10 vol% TEOA	1100	[112]
Bi ₂ MoO ₆ /g-C ₃ N ₄	300 W Xe lamp ($\lambda > 420$ nm)	100 ml 10 vol% TEOA	563.4	[113]
ZnNb ₂ O ₆ /g-C ₃ N ₄	300 W Xenon arc lamp ($\lambda > 420$ nm)	200 ml 20% methanol aqueous solution	340.9	[114]
CdS/g-C ₃ N ₄	$\lambda > 420$ nm	/	216.48	[57]
CuS/g-C ₃ N ₄	300 W Xe lamp ($\lambda > 420$ nm)	200 ml 20 vol% TEOA	17.2	[115]
ZnS/g-C ₃ N ₄	300 W Xe lamp ($\lambda > 420$ nm)	400 ml aqueous solution containing Na ₂ S and Na ₂ SO ₃	713.68	[116]
NiS ₂ /g-C ₃ N ₄	300 W Xe lamp ($\lambda > 420$ nm)	100 ml 10 vol% TEOA	715.83	[117]
NiS/g-C ₃ N ₄	500 W Xe lamp	450 ml 10 vol% glycerol	3428.57	[118]
MoS ₂ /g-C ₃ N ₄	300 W Xe amp ($\lambda > 420$ nm)	120 ml 25 vol% methanol	132.68	[119]
CoS ₂ /g-C ₃ N ₄	$\lambda > 420$ nm	/	1232	[120]
ZnIn ₂ S ₄ /g-C ₃ N ₄	300 W Xe lamp ($\lambda > 420$ nm)	100 ml 10 vol% TEOA	7740	[121]
Cu ₃ P/g-C ₃ N ₄	300 W Xe lamp	68 ml distilled water and 12 ml TEOA	159.41	[122]
Ni ₂ P/g-C ₃ N ₄	300 W Xe lamp	100 ml 10 vol% TEOA	3344	[123]
FeP/g-C ₃ N ₄	300 W Xe lamp ($\lambda > 420$ nm)	150 ml 10 vol% TEOA	177.9	[124]
MoP/g-C ₃ N ₄	300 W Xe lamp ($\lambda > 420$ nm)	100 ml 10 vol% TEOA	327.5	[125]
CoP/g-C ₃ N ₄	300 W Xe lamp $\lambda > 320$ nm	/	201.5	[126]
g-C ₃ N ₄ /NiCoP	300 W Xe lamp ($\lambda \geq 420$ nm)	100 ml 10 vol% TEOA and 1 mmol/L EY	7690	[127]

via a precipitation method [62]. They found that the H₂ generation yield on Ni(OH)₂/TaON reached 3.15 $\mu\text{mol h}^{-1}$, which was greater than that obtained 0.5 wt% Pt/TaON (1.48 $\mu\text{mol h}^{-1}$). Qi et al. firstly prepared a 1-D Ta₃N₅/BaTaO₂N (BTON) heterostructure via a facile one-step ammonia thermal pathway by using single-phase KBa₂Ta₅O₁₅ (KBTO) as the precursor [63]. This heterostructure showed an absorption edge at 600 nm. The special interface and increscent surface area provided a large number of channels for electron transfer and charge separation, which remarkably improved the H₂ generation yield of Ta₃N₅/BaTaO₂N (4.8 $\mu\text{mol h}^{-1}$, higher than those of bare Ta₃N₅ and BTON nanoparticles).

Li and co-authors summarized the recent advances in H₂ generation on nickel-based photocatalysts (noble co-catalysts are also included) [15]. Modification strategies such as enhancing the light capture rate, improving the charge separation/transport, and reinforcing the interfacial interaction of semiconductor/co-catalyst assemblies were discussed in detail, providing new pathways for designing high-activity and high-stability nickel-based photocatalysts for H₂ evolution. The methods used for enhancing the light trapping rate of photocatalysts include designing hierarchical photocatalysts, using surface sensitization, and developing broad-spectrum catalysts. For example, Zhang et al. used a solvothermal route to prepare core-shell TiO₂ nanothorns/C nanofiber photocatalysts [64], which exhibited 13.5 times higher H₂ generation rate than that of doped NiS. The separation of photogenerated carriers in photocatalysts can be improved by constructing Schottky junctions or semiconductor heterojunctions. Li et al. immobilized NiS on g-C₃N₄/C black Schottky junctions and achieved a H₂ generation efficiency of 992 $\mu\text{mol g}^{-1} \text{h}^{-1}$ [131]. Strengthening the interfacial interactions (increase interface contact area or tightness) is another approach to improve the H₂ generation efficiency of photocatalysts. He et al. reported a g-C₃N₄ nanosheet/NiS heterojunction with a close-contact interface via one-step in-situ calcination of urea, thiourea, and nickel acetate. This heterojunction exhibited a maximum H₂ yield of 29.68 $\mu\text{mol h}^{-1}$ [132].

4. Conclusions and future perspectives

Photocatalytic water splitting is the simplest approach to robustly convert and utilize the abundant solar energy to produce H₂, which is a promising and green alternative to fossil fuels. Intensive efforts have

been made to improve the H₂ evolution efficiency of the commonly used photocatalysts for practical applications. This review mainly focuses on the H₂ evolution of high-performance photocatalysts without precious metals. Five types of non-noble metal photocatalysts including metal oxide-based, metal sulfide-based, metal phosphide-based, metal-free, and other non-precious metal photocatalysts have been comprehensively reviewed. Various strategies used for enhancing the photocatalytic H₂ generation from water splitting involving (1) metal or metalloid (non-metal) doping, (2) ion co-doping, (3) establishing heterojunctions (p-n type or Z-scheme), (4) constructing core-shell structures, (5) constructing ternary systems, (6) dye-sensitization, (7) controlling the morphology of the catalysts, and (8) increasing the contact area and strength of the interface have been discussed in detail. It should be noted that high H₂ evolution efficiency can be achieved on photocatalysts without noble metals (even greater than those on the photocatalysts containing precious metals). Unlike noble metal photocatalysts, which deactivate in the presence of contaminants, non-noble metal photocatalysts exhibit high stability even in the presence of contaminants.

Considerable progress has been achieved in improving the H₂ evolution efficiency of photocatalysts. However, the photocatalysts developed till date are not suitable for large-scale practical applications. The challenges for large-scale H₂ generation on photocatalysts without noble metals should not be ignored. (1) The long-term stability of the catalysts. The generally used photocatalysis loop tests are limited to several cycles, and long-term testing based on months or years is hardly reported. This makes it difficult to comment on the industrial applicability of present-day non-noble metal photocatalysts. (2) Low utilization of sunlight. Various approaches such as composition engineering have been used to expand the light absorption range. However, it is still a challenge to achieve solar-driven photocatalytic H₂ evolution. (3) Rapid annihilation of electron-hole pairs. Although approaches, for instance, the construction of the Schottky barrier, p-n junctions, and heterojunctions have been proposed to improve the charge separation of non-noble-metal photocatalysts, significant progress has not been achieved in this regard. (4) The cost of the photocatalyst is always a challenge for its practical applications. (5) The low efficiency or deactivation of photocatalysts in the presence of contaminants.

It should be noted that photocatalytic H₂ generation on non-noble

metal photocatalyst is desirable for practical applications because of their low expense and high efficiency. Further efforts should be made to obviously augment the H₂ generation behavior of non-noble metal catalysts. The kinetics of catalytic reactions, active sites, and reaction routes should be investigated both theoretically and experimentally. DFT calculation is a good auxiliary tool to investigate the reaction barrier and adsorption energy of H₂, which will provide an insight into the reaction mechanism. Multi-disciplinary strategies such as facet engineering, hierarchical structure design, heterojunction construction, and surface/interface engineering should also be investigated comprehensively in order to design and fabricate novel solar-driven non-noble metal photocatalysts. Finally, more attention should be paid to develop new sources for photocatalytic H₂ generation such as wastewater in order to realize the conversion of waste to H₂. This will address both the energy- and environment-related concerns. Recently, Wang et al. realized the co-production of H₂ and diesel precursors from methylfurans on Ru-doped ZnIn₂S₄ under visible light [133], which opened a new pathway for producing biomass/hydrogen energy. The use of non-noble-metal photocatalysts may prominently accelerate H₂ generation from photocatalysis.

Declaration of competing interest

The authors declare that they have no known competing financial interests or personal relationships that could have appeared to influence the work reported in this paper.

Acknowledgements

This work was financially supported by Zhejiang Provincial Natural Science Foundation of China (No. LY17E020008), Technology Foundation for Selected Overseas Chinese Scholar of Zhejiang Province, Fundamental Research Funds for the Provincial Universities of Zhejiang (2020YW53) and Hydrogen Energy Innovation Technology Development Program of the National Research Foundation of Korea (NRF) funded by the Korean government (Ministry of Science and ICT(MSIT)) (NRF-2019M3E6A1064197).

References

- [1] Cheng L, Xiang Q, Liao Y, Zhang H. CdS-Based photocatalysts. *Energy Environ Sci* 2018;11(6):1362–91.
- [2] Sousa SF, Souza BL, Barros CL, Patrocínio AOT. Inorganic photochemistry and solar energy harvesting: current developments and challenges to solar fuel production. *Int J Photoenergy* 2019;23.
- [3] Xu Y, Xu R. Nickel-based cocatalysts for photocatalytic hydrogen production. *Appl Surf Sci* 2015;351:779–93.
- [4] Balat M. Possible methods for hydrogen production. *Energy Sources, Part A Recovery, Util Environ Eff* 2009;31(1):39–50.
- [5] Fang SY, Hu YH. Recent progress in photocatalysts for overall water splitting. *Int J Energy Res* 2019;43(3):1082–98.
- [6] Ren NQ, Cao GL, Wang AJ, Lee DJ, Guo WQ, Zhu YH. Dark fermentation of xylose and glucose mix using isolated Thermoanaerobacterium thermosaccharolyticum W16. *Int J Hydrogen Energy* 2008;33(21):6124–32.
- [7] Khetkorn W, Rastogi RP, Incharoensakdi A, Lindblad P, Madamwar D, Pandey A, Larroche C. Microalgal hydrogen production - a review. *Bioresour Technol* 2017;243:1194–206.
- [8] Acar C, Dincer I, Naterer GF. Review of photocatalytic water-splitting methods for sustainable hydrogen production. *Int J Energy Res* 2016;40(11):1449–73.
- [9] Fujishima A, Honda K. Electrochemical photolysis of water at a semiconductor electrode. *Nature* 1972;238(5358):37–8.
- [10] Kahng S, Yoo H, Kim JH. Recent advances in earth-abundant photocatalyst materials for solar H₂ production. *Adv Powder Technol* 2020;31(1):11–28.
- [11] Pareek V, Bhargava A, Gupta R, Jain N, Panwar J. Synthesis and applications of noble metal nanoparticles: a review. *Adv Sci Eng Med* 2017;9(7):527–44.
- [12] Xie YP, Wang GS, Zhang EL, Zhang X. Photocatalytic hydrogen evolution from water splitting using semiconductors: advance, challenge and prospects. *Chin J Inorg Chem* 2017;33(2):177–209.
- [13] Kudo A, Misaki Y. Heterogeneous photocatalyst materials for water splitting. *Chem Soc Rev* 2009;38(1):253–78.
- [14] Gao T, Chen Z, Huang Q, Niu F, Huang X, Qin L, Huang Y. A Review: preparation of bismuth ferrite nanoparticles and its applications in visible-light induced photocatalyses. *Rev Adv Mater Sci* 2015;40(2):97–109.
- [15] Rongchen Shen JX, Xiang Quanjun, Chen Xiaobo, Jiang Jizhou, Li Xin. Ni-based photocatalytic H₂-production cocatalysts. *Chin J Catal* 2019;40(3):240–88.
- [16] Kong C, Li Z, Lu GX. The dual functional roles of Ru as co-catalyst and stabilizer of dye for photocatalytic hydrogen evolution. *Int J Hydrogen Energy* 2015;40(17): 5824–30.
- [17] Kang HW, Lim SN, Song D, Park SB. Organic-inorganic composite of g-C₃N₄-SrTiO₃: Rh photocatalyst for improved H₂ evolution under visible light irradiation. *Int J Hydrogen Energy* 2012;37(16):11602–10.
- [18] Bai S, Xie ML, Kong Q, Jiang WY, Qiao R, Li ZQ, Jiang J, Xiong YJ. Incorporation of Pd into Pt Co-catalysts toward enhanced photocatalytic water splitting. *Part Part Syst Char* 2016;33(8):6.
- [19] Yang Q, Jones W, Wells PP, Morgan D, Dong LC, Hu BS, Dimitratos N, Dong MD, Bowker M, Besenbacher F, Su R, Hutchings G. Exploring the mechanisms of metal co-catalysts in photocatalytic reduction reactions: is Ag a good candidate? *Appl Catal a-Gen* 2016;518:213–20.
- [20] Li XG, Bi WT, Zhang L, Tao S, Chu WS, Zhang Q, Luo Y, Wu CZ, Xie Y. Single-atom Pt as Co-catalyst for enhanced photocatalytic H₂ evolution. *Adv Mater* 2016;28 (12):2427–31.
- [21] Shen PC, Zhao S, Su D, Li Y, Orlov A. Outstanding activity of sub-nm Au clusters for photocatalytic hydrogen production. *Appl Catal B Environ* 2012;126:153–60.
- [22] Taherinia M, Nasiri M, Abedini E, Pouretedal HR. Comparing the photocatalytic activity of N-doped and S-doped titanium dioxide nanoparticles for water splitting under sunlight radiation. *J Iran Chem Soc* 2018;15(6):1301–10.
- [23] Jia GR, Wang Y, Cui XQ, Zheng WT. Highly carbon-doped TiO₂ derived from MXene boosting the photocatalytic hydrogen evolution. *ACS Sustainable Chem Eng* 2018;6(10):13480–6.
- [24] Niu M, Zhang J, Cao DPI. N-codoping modification of TiO₂ for enhanced photoelectrochemical H₂O splitting in visible-light region. *J Phys Chem C* 2017; 121(47):26202–8.
- [25] Sun T, Fan J, Liu EZ, Liu LS, Wang Y, Dai HZ, Yang YH, Hou WQ, Hu XY, Jiang ZY. Fe and Ni co-doped TiO₂ nanoparticles prepared by alcohol-thermal method: application in hydrogen evolution by water splitting under visible light irradiation. *Powder Technol* 2012;228:210–8.
- [26] Xiao Y, Yu X, Gao Y, Liu JW, Li ZH. Synthesis of Ti³⁺ and P⁵⁺ co-doped TiO₂ nanocrystal with enhanced visible light photocatalytic activity. *Catal Commun* 2017;102:1–4.
- [27] Fujita S, Kawamori H, Honda D, Yoshida H, Arai M. Photocatalytic hydrogen production from aqueous glycerol solution using NiO/TiO₂ catalysts: effects of preparation and reaction conditions. *Appl Catal B Environ* 2016;181:818–24.
- [28] Li CL, Yuan JA, Han BY, Jiang L, Shangguan WF. TiO₂ nanotubes incorporated with CdS for photocatalytic hydrogen production from splitting water under visible light irradiation. *Int J Hydrogen Energy* 2010;35(13):7073–9.
- [29] Zhu YX, Wang YF, Chen Z, Qin LS, Yang LB, Zhu L, Tang P, Gao T, Huang YX, Sha ZL, Tang G. Visible light induced photocatalysis on CdS quantum dots decorated TiO₂ nanotube arrays. *Appl Catal a-Gen* 2015;498:159–66.
- [30] Han H, Kim KM, Lee CW, Lee CS, Pawar RC, Jones JL, Hong YR, Ryu JH, Song T, Kang SH, Choi H, Mhin S. Few-layered metallic 1T-MoS₂/TiO₂ with exposed (001) facets: two-dimensional nanocomposites for enhanced photocatalytic activities. *Phys Chem Chem Phys* 2017;19(41):28207–15.
- [31] Huang JS, Shi ZS, Dong XF. Nickel sulfide modified TiO₂ nanotubes with highly efficient photocatalytic H₂ evolution activity. *J Energy Chem* 2016;25(1):136–40.
- [32] Gomathisankar P, Noda T, Katsumata H, Suzuki T, Kaneko S. Enhanced hydrogen production from aqueous methanol solution using TiO₂/Cu as photocatalysts. *Front Chem Sci Eng* 2014;8(2):197–202.
- [33] Hsu MH, Chang CJ. S-doped ZnO nanorods on stainless-steel wire mesh as immobilized hierarchical photocatalysts for photocatalytic H₂ production. *Int J Hydrogen Energy* 2014;39(29):16524–33.
- [34] Huo JP, Fang LT, Lei YL, Zeng GC, Zeng HP. Facile preparation of yttrium and aluminum co-doped ZnO via a sol-gel route for photocatalytic hydrogen production. *J Mater Chem* 2014;2(29):11040–4.
- [35] Wang J, Xia Y, Zhao H, Wang G, Xiang L, Xu J, Komarneni S. Oxygen defects-mediated Z-scheme charge separation in g-C₃N₄/ZnO photocatalysts for enhanced visible-light degradation of 4-chlorophenol and hydrogen evolution. *Appl Catal B Environ* 2017;206:406–16.
- [36] Yuan YJ, Wang F, Hu B, Lu HW, Yu ZT, Zou ZG. Significant enhancement in photocatalytic hydrogen evolution from water using a MoS₂ nanosheets-coated ZnO heterostructure photocatalyst. *Dalton Trans* 2015;44(24):10997–1003.
- [37] Ma DD, Shi JW, Zou YJ, Fan ZY, Ji X, Niu CM. Highly efficient photocatalyst based on a CdS quantum dots/ZnO nanosheets 0D/2D heterojunction for hydrogen evolution from water splitting. *ACS Appl Mater Interfaces* 2017;9(30): 25377–86.
- [38] Yanalak G, Ajabour A, Aslan E, Ozel F, Patir IH. A systematic comparative study of the efficient co-catalyst-free photocatalytic hydrogen evolution by transition metal oxide nanofibers. *Int J Hydrogen Energy* 2018;43(36):17185–94.
- [39] Ma S, Deng YP, Xie J, He KL, Liu W, Chen XB, Li X. Noble-metal-free Ni₃C cocatalysts decorated CdS nanosheets for high efficiency visible-light-driven photocatalytic H₂ evolution. *Appl Catal B Environ* 2018;227:218–28.
- [40] Lang D, Cheng F, Xiang Q. Enhancement of photocatalytic H₂ production activity of CdS nanorods by cobalt-based cocatalyst modification. *Catal Sci Technol* 2016; 6(16):6207–16.
- [41] Meng A, Zhu B, Bo Z, Zhang L, Bei C. Direct Z-scheme TiO₂/CdS hierarchical photocatalyst for enhanced photocatalytic H₂-production activity. *Appl Surf Sci* 2017;422. S0169433217316720.
- [42] Yu XL, Du RF, Li BY, Zhang YH, Liu HJ, Qu JH, An XQ. Biomolecule-assisted self-assembly of CdS/MoS₂/graphene hollow spheres as high-efficiency

- photocatalysts for hydrogen evolution without noble metals. *Appl Catal B Environ* 2016;182:504–12.
- [43] Lee G-J, Anandan S, Masten SJ, Wu JJ. Photocatalytic hydrogen evolution from water splitting using Cu doped ZnS microspheres under visible light irradiation. *Renew Energy* 2016;89:18–26.
- [44] Lee GJ, Chen HC, Wu JJ. (In, Cu) Co-doped ZnS nanoparticles for photoelectrochemical hydrogen production. *Int J Hydrogen Energy* 2019;44(1): 110–7.
- [45] Dong Z, Wu Y, Thirugnanam N, Li G. Double Z-scheme ZnO/ZnS/g-C₃N₄ ternary structure for efficient photocatalytic H₂ production. *Appl Surf Sci* 2018;430: 293–300.
- [46] Reddy NL, Rao VN, Kumari MM, Sathish M, Venkatakrishnan SM. Development of high quantum efficiency CdS/ZnS core/shell structured photocatalyst for the enhanced solar hydrogen evolution. *Int J Hydrogen Energy* 2018;43(49): 22315–28.
- [47] Huang ZF, Song JJ, Li K, Tahir M, Wang YT, Pan L, Wang L, Zhang XW, Zou JJ. Hollow cobalt-based bimetallic sulfide polyhedra for efficient all-pH-value electrochemical and photocatalytic hydrogen evolution. *J Am Chem Soc* 2016; 138(4):1359–65.
- [48] Li Y, Jin Z, Liu H, Wang H, Zhang Y, Wang G. Unique photocatalytic activities of transition metal phosphide for hydrogen evolution. *J Colloid Interface Sci* 2019; 541:287–99.
- [49] Man HW, Tsang CS, Li MMJ, Mo JY, Huang BL, Lee LYS, Leung YC, Wong KY, Tsang SCE. Transition metal-doped nickel phosphide nanoparticles as electro- and photocatalysts for hydrogen generation reactions. *Appl Catal B Environ* 2019; 242:186–93.
- [50] Li S, Tan J, Jiang Z, Wang J, Li Z. MOF-derived bimetallic Fe-Ni-P nanotubes with tunable compositions for dye-sensitized photocatalytic H₂ and O₂ production. *Chem Eng J* 2020;384:1385–8947.
- [51] Song Y, Xin X, Guo S, Zhang Y, Yang L, Wang B, Li X. One-step MOFs-assisted synthesis of intimate contact MoP-Cu3P hybrids for photocatalytic water splitting. *Chem Eng J* 2020;384:1385–8947.
- [52] Zhou Y, Zhang L, Huang W, Kong Q, Fan X, Wang M, Shi J. N-doped graphitic carbon-incorporated g-C₃N₄ for remarkably enhanced photocatalytic H₂ evolution under visible light. *Carbon* 2016;99:111–7.
- [53] Wang YX, Wang H, Chen FY, Cao F, Zhao XH, Meng SG, Cui YJ. Facile synthesis of oxygen doped carbon nitride hollow microsphere for photocatalysis. *Appl Catal, B* 2017;206:417–25.
- [54] Cui YJ, Wang H, Yang CF, Li M, Zhao YM, Chen FY. Post-activation of in situ B-F codoped g-C₃N₄ for enhanced photocatalytic H₂ evolution. *Appl Surf Sci* 2018; 441:621–30.
- [55] Zhu M, Kim S, Mao L, Fujitsuka M, Zhang J, Wang X, Majima T. Metal-free photocatalyst for H₂ evolution in visible to near-infrared region: black phosphorus/graphitic carbon nitride. *J Am Chem Soc* 2017;139(37):13234–42.
- [56] Yu X, Fan XL, An L, Liu GB, Li ZH, Liu JW, Hu PA. Mesocrystalline Ti3+ + TiO-2 hybridized g-C3N4 for efficient visible-light photocatalysis. *Carbon* 2018;128: 21–30.
- [57] Ji C, Du C, Steinkruger JD, Zhou C, Yang SY. In-situ hydrothermal fabrication of CdS/g-C₃N₄ nanocomposites for enhanced photocatalytic water splitting. *Mater Lett* 2019;240:128–31.
- [58] Tian YM, Ge L, Wang KY, Chai YS. Synthesis of novel MoS₂/g-C₃N₄ heterojunction photocatalysts with enhanced hydrogen evolution activity. *Mater Char* 2014;87:70–3.
- [59] Ye P, Liu XL, Iocozzia J, Yuan YP, Gu LN, Xu GS, Lin ZQ. A highly stable non-noble metal Ni₂P co-catalyst for increased H₂ generation by g-C₃N₄ under visible light irradiation. *J Mater Chem* 2017;5(18):8493–8.
- [60] Wang B, Wang YD. Ieee. Growth of SnO₂ nanosheets on mesoporous SiC nanofibers for enhanced photocatalytic H₂ evolution. New York: Ieee; 2016. p. 383–6.
- [61] Wang B, Zhang JT, Huang F. Enhanced visible light photocatalytic H₂ evolution of metal-free g-C₃N₄/SiC heterostructured photocatalysts. *Appl Surf Sci* 2017;391: 449–56.
- [62] Chen W, Chu MC, Gao L, Mao LQ, Yuan J, Shangguan WF. Ni(OH)₂ loaded on TaON for enhancing photocatalytic water splitting activity under visible light irradiation. *Appl Surf Sci* 2015;324:432–7.
- [63] Qi Y, Chen SS, Li MR, Ding Q, Li Z, Cui JY, Dong BB, Zhang FX, Li C. Achievement of visible-light-driven Z-scheme overall water splitting using barium-modified Ta₃N₅ as a H₂-evolving photocatalyst. *Chem Sci* 2017;8(1):437–43.
- [64] Zhang X, Chen YJ, Xiao YT, Zhou W, Tian GH, Fu HG. Enhanced charge transfer and separation of hierarchical hydrogenated TiO₂ nanothorns/carbon nanofibers composites decorated by NiS quantum dots for remarkable photocatalytic H₂ production activity. *Nanoscale* 2018;10(8):4041–50.
- [65] Humayun M, Raziq F, Khan A, Luo W. Modification strategies of TiO₂ for potential applications in photocatalysis: a critical review. *Green Chem Lett Rev* 2018;11(2):86–102.
- [66] Mohamed MA, Zain MFM, Minggu LJ, Kassim MB, Jaafar J, Amin NAS, Ng YH. Revealing the role of kapok fibre as bio-template for In-situ construction of C-doped g-C₃N₄@C, N co-doped TiO₂ core-shell heterojunction photocatalyst and its photocatalytic hydrogen production performance. *Appl Surf Sci* 2019;476: 205–20.
- [67] Ge MZ, Cai JS, Iocozzia J, Cao CY, Huang JY, Zhang XN, Shen JL, Wang SC, Zhang SN, Zhang KQ, Lai Y, Lin K, Q Z. A review of TiO₂ nanostructured catalysts for sustainable H₂ generation. *Int J Hydrogen Energy* 2017;42(12):8418–49.
- [68] Wang WK, Xu DF, Cheng B, Yu JG, Jiang CJ. Hybrid carbon@TiO₂ hollow spheres with enhanced photocatalytic CO₂ reduction activity. *J Mater Chem* 2017;5(10): 5020–9.
- [69] Ge MZ, Li QS, Cao CY, Huang JY, Li SH, Zhang SN, Chen Z, Zhang KQ, Al-Deyab SS, Lai YK. One-dimensional TiO₂ nanotube photocatalysts for solar water splitting. *Adv Sci* 2017;4(1):31.
- [70] Sajan CP, Wageh S, Al-Ghamdi AA, Yu JG, Cao SW. TiO₂ nanosheets with exposed {001} facets for photocatalytic applications. *Nano Research* 2016;9(1):3–27.
- [71] Nakata K, Fujishima A. TiO₂ photocatalysis: design and applications. *J Photochem Photobiol, A* 2012;13(3):169–89.
- [72] Kho YK, Iwase A, Teoh WY, Mäder L, Kudo A, Amal R. Photocatalytic H₂ evolution over TiO₂ nanoparticles. The synergistic effect of anatase and rutile. *J Phys Chem C* 2010;114(6):2821–9.
- [73] Liu N, Häublein V, Zhou X, Venkatesan U, Hartmann M, Mackovic M, Nakajima T, Spiecker E, Osvet A, Frey L. “Black” TiO₂ nanotubes formed by high-energy proton implantation show noble-metal-co-catalyst free photocatalytic H₂-evolution. *Nano Lett* 2015;15(10):6815–20.
- [74] Gao C, Wei T, Zhang Y, Song X, Huan Y, Liu H, Zhao M, Yu J, Chen X. A photoresponsive rutile TiO₂ heterojunction with enhanced electron-hole separation for high-performance hydrogen evolution. *Adv Mater* 2019;31(8): 1806596.
- [75] Ge M-Z, Cao C-Y, Li S-H, Tang Y-X, Wang L-N, Qi N, Huang J-Y, Zhang K-Q, Al-Deyab SS, Lai Y-K. In situ plasmonic Ag nanoparticle anchored TiO₂ nanotube arrays as visible-light-driven photocatalysts for enhanced water splitting. *Nanoscale* 2016;8(9):5226–34.
- [76] Zhou W, Li W, Wang J-Q, Qu Y, Yang Y, Xie Y, Zhang K, Wang L, Fu H, Zhao D. Ordered mesoporous black TiO₂ as highly efficient hydrogen evolution photocatalyst. *J Am Chem Soc* 2014;136(26):9280–3.
- [77] Amano F, Nakata M, Yamamoto A, Tanaka T. Rutile titanium dioxide prepared by hydrogen reduction of Degussa P25 for highly efficient photocatalytic hydrogen evolution. *Catal Sci Technol* 2016;6(14):5693–9.
- [78] Hu Q, Li J, Li Q, Wang G, Huang J, Huang X. One-step synthesis of nonstoichiometric TiO₂ nanorod films for enhanced photocatalytic H₂ evolution. *Dalton Trans* 2018;47(13):4478–85.
- [79] Shi S, Chen Y, Lee J, Jiang Z, Cui X. Direct fabrication of anatase TiO₂ hollow microspheres for applications in photocatalytic hydrogen evolution and lithium storage. *J Solid State Electrochem* 2018;22(3):705–15.
- [80] Liu N, Zhou X, Nguyen NT, Peters K, Zoller F, Hwang I, Schneider C, Miehlich ME, Freitag D, Meyer K. Black magic in gray titania: noble-metal-free photocatalytic H₂ evolution from hydrogenated anatase. *Chem Sus Chem* 2017;10(1):62–7.
- [81] Cheng G, Wei Y, Xiong J, Gan Y, Zhu J, Xu F. Same titanium glycolate precursor but different products: successful synthesis of twinned anatase TiO₂ nanocrystals with excellent solar photocatalytic hydrogen evolution capability. *Inorg Chem Front* 2017;4(8):1319–29.
- [82] Zhao M, Xu H, Chen H, Ouyang S, Umezawa N, Wang D, Ye J. Photocatalytic reactivity of {121} and {211} facets of brookite TiO₂ crystals. *J Mater Chem* 2015;3(5):2331–7.
- [83] Masolo E, Senes N, Pellicer E, Baró MD, Enzo S, Pilo MI, Mulas G, Garroni S. Evaluation of the anatase/rutile phase composition influence on the photocatalytic performances of mesoporous TiO₂ powders. *Int J Hydrogen Energy* 2015;40(42):14483–91.
- [84] Alsalki Y, Hakki A, Schneider J, Bahnemann DW. Co-catalyst-free photocatalytic hydrogen evolution on TiO₂: synthesis of optimized photocatalyst through statistical material science. *Appl Catal B Environ* 2018;238:422–33.
- [85] Zhang W, He H, Tian Y, Lan K, Liu Q, Wang C, Liu Y, Elzahary A, Che R, Li W. Synthesis of uniform ordered mesoporous TiO₂ microspheres with controllable phase junctions for efficient solar water splitting. *Chem Sci* 2019;10(6):1664–70.
- [86] Wierzbicka E, Zhou X, Denisov N, Yoo J, Fehn D, Liu N, Meyer K, Schmuki P. Self-enhancing H₂ evolution from TiO₂ nanostructures under illumination. *Chem Sus Chem* 2019;12(9):1900–5.
- [87] Liu Z, Zheng Y, Gao T, Zhang J, Sun X, Zhou G. Fabrication of anatase TiO₂ tapered tetragonal nanorods with designed {100}, {001} and {101} facets for enhanced photocatalytic H₂ evolution. *Int J Hydrogen Energy* 2017;42(34): 21775–85.
- [88] Wang Y, Zhou M, He Y, Zhou Z, Sun Z. In situ loading CuO quantum dots on TiO₂ nanosheets as cocatalyst for improved photocatalytic water splitting. *J Alloys Compd* 2020;813:152184.
- [89] Zhou DT, Chen Z, Yang Q, Dong XP, Zhang JJ, Qin LS. In-situ construction of all-solid-state Z-scheme g-C₃N₄/TiO₂ nanotube arrays photocatalyst with enhanced visible-light-induced properties. *Sol Energy Mater Sol Cells* 2016;157:399–405.
- [90] Zhou DT, Chen Z, Yang Q, Shen C, Tang G, Zhao SL, Zhang JJ, Chen D, Wei QH, Dong XP. Facile construction of g-C₃N₄ nanosheets/TiO₂ nanotube Arrays as Z-scheme photocatalyst with enhanced visible-light performance. *ChemCatChem* 2016;8(19):3064–73.
- [91] Zhou DT, Chen Z, Gao T, Niu F, Qin LS, Huang YX. Hydrogen generation from water splitting on TiO₂ nanotube-array-based photocatalysts. *Energy Technol* 2015;3(9):888–95.
- [92] Bunn CW. The lattice-dimensions of zinc oxide. *Proc Phys Soc* 2002;47(5): 835–42.
- [93] Tsukazaki A, Yuji H, Akasaka S, Tamura K, Nakahara K, Tanabe T, Takasu H, Ohtomo A, Kawasaki M. High electron mobility exceeding 104 cm² V⁻¹ s⁻¹ in Mg_xZn_{1-x}O/ZnO single heterostructures grown by molecular beam epitaxy. *Appl phys express* 2008;1(5): 1882–0786.
- [94] Krasienapibal TS, Fukumura T, Hirose Y, Hasegawa T. Improved room temperature electron mobility in self-buffered anatase TiO₂ epilayer thin film grown at low temperature. *Jpn J Appl Phys* 2014;53(9):1347–4065.
- [95] Qi KZ, Cheng B, Yu JG, Ho WK. Review on the improvement of the photocatalytic and antibacterial activities of ZnO. *J Alloys Compd* 2017;727:792–820.

- [96] Zhang K, Guo LJ. Metal sulphide semiconductors for photocatalytic hydrogen production. *Catal Sci Technol* 2013;3(7):1672–90.
- [97] Cheng C, Zong S, Shi J, Xue F, Zhang Y, Guan X, Zheng B, Deng J, Guo L. Facile preparation of nanosized MoP as cocatalyst coupled with g-C₃N₄ by surface bonding state for enhanced photocatalytic hydrogen production. *Appl Catal, B* 2020;118620.
- [98] Sun Z, Zhu M, Lv X, Liu Y, Shi C, Dai Y, Wang A, Majima T. Insight into iron group transition metal phosphides (Fe₂P, Co₂P, Ni₂P) for improving photocatalytic hydrogen generation. *Appl Catal, B* 2019;246:330–6.
- [99] Cheng L, Xie S, Zou Y, Ma D, Sun D, Li Z, Wang Z, Shi J. Noble-metal-free Fe₂P–Co₂P co-catalyst boosting visible-light-driven photocatalytic hydrogen production over graphitic carbon nitride: the synergistic effects between the metal phosphides. *Int J Hydrogen Energy* 2019;44(8):4133–42.
- [100] Jian Q, Jin Z, Wang H, Zhang Y, Wang G. Photoelectron directional transfer over a g-C₃N₄/CdS heterojunction modulated with WP for efficient photocatalytic hydrogen evolution. *Dalton Trans* 2019;48(13):4341–52.
- [101] Wang X, Maeda K, Thomas A, Takanabe K, Xin G, Carlsson JM, Domen K, Antonietti M. A metal-free polymeric photocatalyst for hydrogen production from water under visible light. *Nat Mater* 2009;8(1):76–80.
- [102] Thaweesak S, Lyu M, Peerakiatkhajohn P, Butburee T, Luo B, Chen H, Wang L. Two-dimensional g-C₃N₄/Ca₂Nb₂TaO₁₀ nanosheet composites for efficient visible light photocatalytic hydrogen evolution. *Appl Catal B Environ* 2017;202:184–90.
- [103] Chen Z, Lu S, Wu Q, He F, Zhao N, He C, Shi C. Salt-assisted synthesis of 3D open porous g-C₃N₄ decorated with cyano groups for photocatalytic hydrogen evolution. *Nanoscale* 2018;10(6):3008–13.
- [104] Wang W, Zhu S, Zhou J, Li T, Ping D, Zhao Z, Tan Y, Cong X, Shuai C. Halloysite-derived mesoporous g-C₃N₄ nanotubes for improved visible-light photocatalytic hydrogen evolution. *Appl Clay Sci* 2018;158:143–9.
- [105] Wang M, Ju P, Zhao Y, Li JJ, Han XX, Hao ZM. In situ ion exchange synthesis of MoS₂/g-C₃N₄ heterojunctions for highly efficient hydrogen production. *New J Chem* 2018;42(2):910–7.
- [106] Liu WS, Wang LC, Chin TK, Yen YC, Perng TP. Fabrication of TiO₂ on porous g-C₃N₄ by ALD for improved solar-driven hydrogen evolution. *RSC Adv* 2018;8(54):30642–51.
- [107] Guo F, Shi WL, Zhu C, Li H, Kang ZH. CoO and g-C₃N₄ complement each other for highly efficient overall water splitting under visible light. *Appl Catal, B* 2018;226:412–20.
- [108] Ji C, Yin SN, Sun SS, Yang SY. An in-situ mediator-free route to fabricate Cu₂O/g-C₃N₄ type-II heterojunctions for enhanced visible-light photocatalytic H₂ generation. *Appl Surf Sci* 2018;434:1224–31.
- [109] Shi JW, Cheng C, Hu YC, Liu MC, Guo LJ. One-pot preparation of porous Cr₂O₃/g-C₃N₄ composites towards enhanced photocatalytic H₂ evolution under visible-light irradiation. *Int J Hydrogen Energy* 2017;42(7):4651–9.
- [110] Huang Q-Z, Wang J-C, Wang P-P, Yao H-C, Li Z-J. In-situ growth of mesoporous Nb₂O₅ microspheres on g-C₃N₄ nanosheets for enhanced photocatalytic H₂ evolution under visible light irradiation. *Int J Hydrogen Energy* 2017;42(10):6683–94.
- [111] Hong YZ, Fang ZY, Yin BX, Luo BF, Zhao Y, Shi WD, Li CS. A visible-light-driven heterojunction for enhanced photocatalytic water splitting over Ta₂O₅ modified g-C₃N₄ photocatalyst. *Int J Hydrogen Energy* 2017;42(10):6738–45.
- [112] Zou WX, Deng B, Hu XX, Zhou YP, Pu Y, Yu SH, Ma KL, Sun JF, Wan HQ, Dong L. Crystal-plane-dependent metal oxide-support interaction in CeO₂/g-C₃N₄ for photocatalytic hydrogen evolution. *Appl Catal B Environ* 2018;238:111–8.
- [113] Li J, Yin YC, Liu EZ, Ma YN, Wan J, Fan J, Hu XY. In situ growing Bi₂MoO₆ on g-C₃N₄ nanosheets with enhanced photocatalytic hydrogen evolution and disinfection of bacteria under visible light irradiation. *J Hazard Mater* 2017;321:183–92.
- [114] Yan M, Hua YQ, Zhu FF, Sun L, Gu W, Shi WD. Constructing nitrogen doped graphene quantum dots-ZnNb₂O₆/g-C₃N₄ catalysts for hydrogen production under visible light. *Appl Catal, B* 2017;206:531–7.
- [115] Chen TJ, Song CJ, Fan MS, Hong YZ, Hu B, Yu LB, Shi WD. In-situ fabrication of CuS/g-C₃N₄ nanocomposites with enhanced photocatalytic H₂-production activity via photoinduced interfacial charge transfer. *Int J Hydrogen Energy* 2017;42(17):12210–9.
- [116] Hao XQ, Zhou J, Cui ZW, Wang YC, Wang Y, Zou ZG. Zn-vacancy mediated electron-hole separation in ZnS/g-C₃N₄ heterojunction for efficient visible-light photocatalytic hydrogen production. *Appl Catal B Environ* 2018;229:41–51.
- [117] Li HT, Wang M, Wei YP, Long F. Noble metal-free NiS₂ with rich active sites loaded g-C₃N₄ for highly efficient photocatalytic H₂ evolution under visible light irradiation. *J Colloid Interface Sci* 2019;534:343–9.
- [118] Kadi MW, Mohamed RM, Ismail AA, Bahnamian DW. Decoration of mesoporous graphite-like C₃N₄ nanosheets by NiS nanoparticle-driven visible light for hydrogen evolution. *Appl Nanosci* 2018;8(6):1587–96.
- [119] Liu YZ, Zhang HY, Ke J, Zhang JQ, Tian WJ, Xu XY, Duan XG, Sun HQ, Tade MO, Wang SB, OD (MoS₂)/2D(g-C₃N₄) heterojunctions in Z-scheme for enhanced photocatalytic and electrochemical hydrogen evolution. *Appl Catal B Environ* 2018;228:64–74.
- [120] Li HY, Deng PH, Hou Y. Cobalt disulfide/graphitic carbon nitride as an efficient photocatalyst for hydrogen evolution reaction under visible light irradiation. *Mater Lett* 2018;229:217–20.
- [121] Ding N, Zhang LS, Zhang HY, Shi JJ, Wu HJ, Luo YH, Li DM, Meng QB. Microwave-assisted synthesis of ZnIn₂S₄/g-C₃N₄ heterojunction photocatalysts for efficient visible light photocatalytic hydrogen evolution. *Catal Commun* 2017;10:173–7.
- [122] Shen RC, Xie J, Lu XY, Chen XB, Li X. Bifunctional Cu₃P decorated g-C₃N₄ nanosheets as a highly active and robust visible-light photocatalyst for H₂ production. *ACS Sustainable Chem Eng* 2018;6(3):4026–36.
- [123] Liu EZ, Jin CY, Xu CH, Fan J, Hu XY. Facile strategy to fabricate Ni₂P/g-C₃N₄ heterojunction with excellent photocatalytic hydrogen evolution activity. *Int J Hydrogen Energy* 2018;43(46):21355–64.
- [124] Zeng DQ, Zhou T, Ong WJ, Wu MD, Duan XG, Xu WJ, Chen YZ, Zhu YA, Peng DL. Sub-5 nm ultra-fine FeP nanodots as efficient Co-catalysts modified porous g-C₃N₄ for precious-metal-free photocatalytic hydrogen evolution under visible light. *ACS Appl Mater Interfaces* 2019;11(6):5651–60.
- [125] Liu W, Shen J, Liu QQ, Yang XF, Tang H. Porous MoP network structure as co-catalyst for H₂ evolution over g-C₃N₄ nanosheets. *Appl Surf Sci* 2018;462:822–30.
- [126] Sun XJ, Yang DD, Dong H, Meng XB, Sheng JL, Zhang X, Wei JZ, Zhang FM. ZIF-derived CoP as a cocatalyst for enhanced photocatalytic H₂ production activity of g-C₃N₄. *Sustainable Energy Fuels* 2018;2(6):1356–61.
- [127] Xu JX, Qi YH, Wang WB, Wang L. Montmorillonite-hybridized g-C₃N₄ composite modified by NiCoP cocatalyst for efficient visible-light-driven photocatalytic hydrogen evolution by dye-sensitization. *Int J Hydrogen Energy* 2019;44(8):4114–22.
- [128] Nariki Y, Inoue Y, Tanaka K. Production of ultra-fine SiC powder from SiC bulk by arc-plasma irradiation under different atmospheres and its application to photocatalysts. *J Mater Sci* 1990;25(7):3101–4.
- [129] Hara M, Hitoki G, Takata T, Kondo JN, Kobayashi H, Domen K. TaON and Ta₃N₅ as new visible light driven photocatalysts. *Catal Today* 2003;78(1–4):555–60.
- [130] Hara M, Takata T, Kondo JN, Domen K. Photocatalytic reduction of water by TaON under visible light irradiation. *Catal Today* 2004;89(3):313–7.
- [131] Wen JQ, Xie J, Yang ZH, Shen RC, Li HY, Luo XY, Chen XB, Li X. Fabricating the robust g-C₃N₄ nanosheets/carbon/NiS multiple heterojunctions for enhanced photocatalytic H₂ generation: an insight into the trifunctional roles of nanocarbons. *ACS Sustainable Chem Eng* 2017;5(3):2224–36.
- [132] He KL, Xie J, Li ML, Li X. In situ one-pot fabrication of g-C₃N₄ nanosheets/NiS cocatalyst heterojunction with intimate interfaces for efficient visible light photocatalytic H₂ generation. *Appl Surf Sci* 2018;430:208–17.
- [133] Luo N, Montini T, Zhang J, Fornasiero P, Fonda E, Hou T, Nie W, Lu J, Liu J, Heggen M. Visible-light-driven coproduction of diesel precursors and hydrogen from lignocellulose-derived methylfurans. *Nat Energy* 2019;4(7):575–84.